UNIVERSITY OF TROMSØ UIT

FACULTY OF SCIENCE AND TECHNOLOGY
DEPARTMENT OF PHYSICS AND TECHNOLOGY

Late Holocene climate variability in the North Atlantic realm from paleo data and climate simulations

TINE NILSEN

EOM-3901
Master's Thesis in Energy, Climate and Environment

June 2013

Aknowledgements

I would like to thank my two advisors, Kristoffer Rypdal and Dmitry Divine. They have both helped me find topics, litterature and methods for my thesis. Kristoffer has as my main advisor helped and encouraged me with both general and specific tasks. Dmitry has shared his knowledge on paleo and simulated data in a very instructive way. I appreciate especially that he has taken time to supervise my work during his parental leave. My fellow student Hege Beate Fredriksen and associate professor Martin Rypdal deserves credit as well for all their help. At last, I would also like to thank mr. Eduardo Zorita and Carl-Friedrich Shcleussner for providing simulated data series on personal request from Dmitry.

Abstract

This thesis presents the results of the comparative analysis of surface temperature series from paleoproxy reconstructions and climate simulations. The proxy to model comparison is done using the results from 12 simulations produced by 5 different climate models covering the period of the late Holocene. Agreement between the model results and the paleoproxy reonstrcuctions is analyzed both on the local/regional scale using the paleoproxy series from two marine sediment cores from the northern North Atlantic, and globally with the available multiproxy reconstruction of past Northern Hemispheric temperature. Long term temperature trends, long range memory properties, magnitude of variability at different time scales as inferred from series spectral properties quantify the capability of the models to simulate past climate. Persistence on time scales up to a few hundred years is found for the Hemispheric temperature reconstruction under study, and some of the simulated data sets. Further, linear trend estimates in sea surface temperature records from two regions in the North Atlantic suggest antiphased linear trends for the reconstructed temperature data, which is only reproduced in one of the model experiments. When studying two known temperature anomalies, the medieval warm period and the little ice age, the anomalies are detected in both paleoproxy and simulated temperature time series.

Contents

Chapter 1

Introduction

Over the last decades, climate models of varying complexity have become important tools in climate research. However, the overall complexity of the climate system makes an exact description of the required system variables unattainable, implying the use of various simplifying assumptions. The model capability of reproducing features of the actual climate system therefore require additional assessment. This thesis presents two case studies where the output from climate models and proxy-based reconstructions of past sea surface temperature (SST) and air temperature are used to assess the skills of five different climate models.
First, model simulations of the late Holocene climate are investigated for long range memory (LRM) properties. The sea-surface temperature (SST) record is selected for both regional and Hemispheric data. In contrary to a white noise hypothesis, suggesting the climate process is a realization of an uncorrelated stationary Gaussian process, the LRM theory suggest long-term correlation between observations widely separated in time, associated with slow responses in the climate system. Earlier studies have shown that instrumental and reconstructed SST time series exhibit LRM on time scales from months to centuries, [*Pelletier and Turcotte* (1999), *Rybski et al.* (2006), *Rypdal & Rypdal* (2010), *Rypdal et al.* (2013)].
It is therefore of importance to investigate if model simulations can also reproduce LRM properties on the same time scales. The lack of LRM in the modeled climate would be an indication that there exist some slow responses in the climate system that are not included or not incorporated correctly in the models.

The second part of the thesis shows an example of the so-called proxy-to model intercomparison study. The studies of [*Miettinen et al.* (2012), *Berner et al.* (2011)] use proxy-based reconstructions of sea-surface temperature from two marine sediment cores, and find an indication of antiphased SST variations between eastern and western orthern North Atlantic during the last 2800 years. This study is limited to analysis of long term climate tendency for the two locations, by considering linear trends in model simulations and paleo climate time series. Statistical significance of the trends are tested by using a white noise hypothesis.
By summarizing the analysis results of the climate model time series, an intuitive assessment of parts of the model performance can be achieved.
As a concluding task, the sediment core SST data are assumed to exhibit LRM on time scales up to a few centuries. Linear trends are estimated for the western and eastern North Atlantic Ocean, and significance testing is performed using an LRM hypothesis. This illustrates the different results one can encounter when critically choosing a statistical model for the climate noise.

1.1 Why use the data from climate simulations of the past?

The real climate exhibits a stochastic nature, being a manifestation of a high-dimensional complex system. As a dynamical system, it involves a huge number of variables, processes and feedback mechanisms, and can not be described directly from first physical principles. Hence, climate models involving various simplifications and parametrizations have been developed. They are based on equations describing energy and mass conservation, fluid mechanics and thermodynamics. The spatial and temporal resolution of the models vary, and computation time depends on the degree of model complexity. The atmosphere and the ocean are simulated in separate models, which can be coupled together and connected to models for the terrestrial biosphere, ice sheets, sea ice, the carbon cycle and more. A large number of experiments can be performed with one single model by varying initial conditions, external forcing and parameters.
It is highly unlikely that any realization ever produced from a climate model is

identical to the past, present or future climate of the world. However, the simulations may produce realistic scenarios, which are useful for climate studies. Models can generate global data sets with high temporal resolution, which represent a great advantage in comparison with instrumental and reconstructed data. Instrumental measurements only cover a short time period and selected areas, and there may be data missing within the time series. Reconstructed paleoclimatic data also have limited spatial and temporal coverage, in addition to the uncertanties connected with the different reconstruction methods.

Chapter 2

Theoretical background and motivation

2.1 An introduction to long range memory processes

The nature of a climate variable can be studied in greater detail if it its timeseries is decomposed into a deterministic and a stochastic part, [*Saltzman* (2002)]. The deterministic part include oscillation modes and trends, while the remaining part can be represented by a stochastic process. Different stochastic process models are found to be representative of the noise in a climatic signal, such as the Gaussian and AR(1), [*Rypdal et al.* (2013)]. Note that the decomposition will depend on the chosen stochastic process, due to different memory properties of the processes. The integral of the autocorrelation function C(t) defines the memory property for a stochastic process:

$$\lim_{T\to\infty} \int_0^\infty C(t)\, dx$$

Bounded integral: Short Range Memory (SRM).
Unbounded integral: Long Range Memory (LRM).

Today, the first-order autoreressive model (AR(1)) hypothesis is typically used

to describe climate processes, [*Hasselmann* (1976)]. The AR(1) model has an exponential autocorrelation funtion (ACF) and Lorentzian power spectral density (PSD). To find the integral of the ACF, the discrete time AR(1) process is transformed to its continuous-time analogue; the Ornstein-Uhlenbeck (OU) stochastic process. The evolution of the OU noise in time can be presented as:

$$\frac{\mathrm{dy}}{\mathrm{dt}} = -\frac{\mathrm{y}}{\tau} + \sqrt{\frac{2\sigma^2}{\tau}}\xi(\mathrm{t})$$

Where τ is the correlation time, and $\xi(\mathrm{t})$ is a zero-mean Gaussian white noise.

The Ornstein-Uhlenbeck stochastic process has the character of a Brownian motion on time scales less than τ, and of a white noise on time scales longer than τ, [*Rypdal et al.* (2013)]. The decorrelation time is definite for an OU stochastic process, meaning that the AR(1) process exhibit SRM.

Moving on to LRM stochastic processes, note that they have ACF and PSD with power-law form, [*Malamud & Turcotte* (1998)]:

$$\mathrm{C(t)} \sim \mathrm{t}^{\frac{\beta}{2}-1}, \qquad\qquad \mathrm{S(f)} \sim \mathrm{f}^{-\beta}$$

The choice of the spectral index β yields a family of stochastic processes exhibiting LRM or SRM, where β: $-1 < \beta < 3$

- $-1 < \beta < 0$ is an antipersistent fractional Gaussian noise (fGn). In this case:

  $$\lim_{\mathrm{T}\to\infty} \int_0^{\infty} \mathrm{C(t)}\, \mathrm{dt} = 0$$

  and the process is not considered to exhibit LRM.

- $0 < \beta < 1$ is a persistent (fGn):

  $$\lim_{\mathrm{T}\to\infty} \int_0^{\infty} \mathrm{C(t)}\, \mathrm{dt} = \infty$$

  the process exhibit LRM.

- $1 < \beta > 3$ is a fractional Brownian motion (fBm), where β=2 is a classical Brownian motion.
- The limit β=1 separates stationary from nonstationary processes (fGn from fBm), and is sometimes called "pink noise" or 1/f-noise.

fGns will be in particular focus in this thesis, because previous studies indicate that this is the best statistial model for both global, Hemispheric and regional SST time series, [*Rypdal et al.* (2013)].
A series of identical Gaussian random variables $X_1, X_2 ..... X_N$ with the following property is a fractional Gaussian noise, [*Qian* (2003)]:

$$Y_N = \frac{X_1 + X_2 + ... + X_N}{N^H} \stackrel{d}{=} X$$

where H is the Hurst exponent, $0 < H < 1$, and $\stackrel{d}{=}$ mean equal in distribution. H is connected with the spectral scaling index β in the following manner: $\beta = 2H - 1$. H= 0.5 equals no memory/persistence in the data set, while as H approaches 1 the persistence increases.

A fractional Brownian motion is defined as the partial sum of the fGn, with Hurst exponent H:

$$B_k = X_1 + X_2 + ... + X_k$$

B_k^H is a self-similar [1] process, which exhibit the property:

$$B_k^H, \stackrel{d}{=} \lambda^H \beta_{\lambda k}$$

whwre λ is a constant, and $1 < H < 3$.

[1] Self similarity implies that the behaviour of a phenomenon is identical at different scales

Chapter 3

Data

Paleo climate data from two marine sediment cores in the northern North Atlantic are provided and feature uneven time steps, common for this type of proxy data. The time series cover approximately the last 2800 years, known as the late Holocene period. A temperature reconstruction for the Northern Hemisphere [*Moberg et al.* (2005)] is also analyzed, in order to have Hemispheric paleodata to compare with simulations. Climate simulations from five models of varying complexity are provided for analysis, covering the late Holocene; LOVECLIM, CLIMBER-3α, COSMOS, ECHO-G, and HadCM3.

3.1 Paleoproxy data

Marine sediment cores are widely used for reconstructing past climate. One of the common approaches uses siliceous frustules (shells) from diatoms found within seafloor sediments [*Koç Karpuz & Schrader* (1990)]. Diatoms are unicellular, photosynthetic algae. They live in surface waters from 0-50 m depth [*Miettinen et al.* (2012)]. After death, the organisms fall to the seafloor. Only the hard shells remains after decomposition, which is preserved and buried by sediments.
The general assumption is that the down-core composition of diatomic microfossil assemblages is related with past environmental conditions at the core site. A number of statistical techniques are elaborated to convert assemblages to past estimates of hydrographic conditions, including sea-surface temperature at the study

site.

In the Arctic and sub-Artcic region, the diversity and production of diatoms is high. To study the diatom microfossils, sediment cores are usually recovered in areas with high sedimentation rate to ensure highest possible temporal resolution. Adequate age models for marine sediment cores are based on ^{14}C dating, ^{210}Pb measurements, and ash layers, [*Miettinen et al.* (2012), *Andersen et al.* (2004)]. Sediment cores from one specific location generally include a surface sample (box core) about 1 m^3, and a gravity or piston core sample ranging from a few meters to 20 m in length, depending on the equipment used. The box corer provide undisturbed surface sediments, which have the quality of not being pushed together. The gravity corer and piston corer provide longer samples, where the surface sediments are too compressed to be used, [*Wefer et al.* (2003)]

The cores are cut open and described at the laboratorium. Samples are taken at even distances from top to bottom, and they are weighted, dried and weighted again. The samples are then sieved, and diatom frustules are picked by hand using a microscope.

Specific procedures exist for counting frustules and identifying species, [*Schrader & Gersonde* (1978)]. In general, the temperature and salinity tolerance vary between groups of diatom species, and such properties are unchanged with time. A set of 52 diatom species, from 139 surface samples is used as a modern calibration set from the northern North Atlantic region [*Koç Karpuz & Schrader* (1990)]. The observed SST is known for these samples, and diatom species are categorized into assemblages for the northern North Atlantic, [*Berner et al.* (2011), *Andersen et al.* (2004)]. The assemblages are representative of different regions in the area, with specific watermasses dominating:

(1) Arctic Greenland assemblage, (2) North Atlantic assemblage, (3) Sub-Arctic assemblage, (4) Norwegian Atlantic Current assemblage, (5) Sea Ice assemblage, (6) Arctic assemblage, (7) East- & West Greenland Current assemblage, (8) Mixed Water Masses assemblage.

When diatoms from a sediment core are counted, identified and categorized into the right assemblages, a statistical technique of choice is used to convert downcore diatomic assemblages to SST estimates. The techniques include the regres-

sion analysis of Imbrie & Kipp (I&K) [*Imbrie & Kipp* (1971)], maximum likelihood (ML) [*Walpole et al.* (2007)] and WA-PLS (weighted-average least partial squares) [*ter Braak & Juggins* (1993)]. To validate each statistical method, the core top SST estimates (corresponding to the modern diatom assemblages) are compared with the observed values from the calibration set, [*Andersen et al.* (2004)].
The performance of the three methods mentioned above is tested in [*Berner et al.* (2011)], and WA-PLS is found to give the best fit to the observed SST values. It has a RMSE of 0.75 °C, a coefficient of determination between observed and inferred SST of 0.96, and a maximum bias of 0.44°C. The method can be considered the unimodal-based equivalent of multiple linear regression, and August sea surface temperature (aSST) is found to give the best fit [*Berner et al.* (2008)].

3.1.1 Marine sediment cores and locations

Figure 3.1 shows the two core locations from the eastern and western subpolar North Atlantic considered in this study. Reykjanes Ridge is a section of the Mid-Atlantic Ridge to the southwest of Iceland. The Vøring Plateau is an elevated submarine region in the Norwegian Sea.
Down-core diatomic assemblages are converted to SST estimates by the WA-PLS method. A linear regression analysis is performed in [*Miettinen et al.* (2012)] for the two SST time series. Figure 3.2 and 3.3 show linear trends for both locations, indicating an antiphasing of the two temperature trends. The medieval warm period (MWP 800-1400) and the Little Ice Age (LIA 1400-1900), are the two most prominent climate anomalies in the North Atlantic region during the past millenium. The causes of the anomalies are not fully understood, but a change in heat distribution may have been caused by external forcing [*Schleussner & Feulner* (2012)]. The MWP and LIA climate anomalies are detected for both paleo SST time series, but are antiphased for the two locations. The mechanism driving such an antiphasing between the eastern and western subpolar North Atlantic is poorly understood. If model simulations show similar trends and antiphasing, the dynamics can be investigated in greater detail. This will contribute to a better understanding of the natural climate variabity in the North Atlantic region.

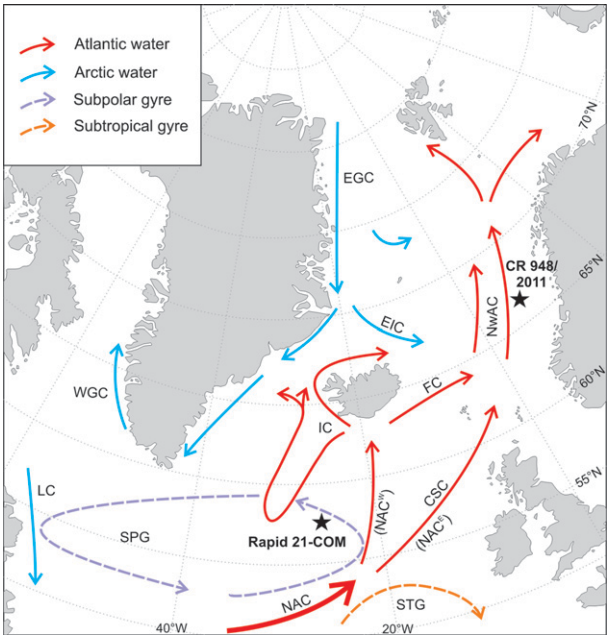

Figure 3.1: *Map of the study area showing the core site locations; Rapid-21-COM at the Reykjanes Ridge and CR 948/2011 at the Vøring Plateau. The modern surface ocean circulation system is shown; NAC^{W,E} (North Atlantic Current, western and eastern branch), IC (Irminger Current), FC (Faroe Current), CSC (Continental Slope Current), NwAC (Norwegian Atlantic Current), EGG (East Greenland Current), EIC (East Icelandic Current), WGC (West Greenland Current), LC (Labrador Current), SPG (subpolar gyre), STG (subtropical gyre)*
[Miettinen et al. (2012)]

Reykjanes Ridge

For the Iceland Basin, composite core Rapid 21-COM is analyzed in [*Miettinen et al.* (2012)]. The core consist of a 54.3 cm long box core, and a 3.725 m long gravity core. The temperature reconstruction has an average resolution of 2 years for year 1770-2000 (box core), 8-10 years for year 800-1770, and 40 years for year 800 BC- AD 800, (both gravity core). Figure 3.2 shows the time series with the estimated linear trend found in the paper; 1 °C over 2800 years.

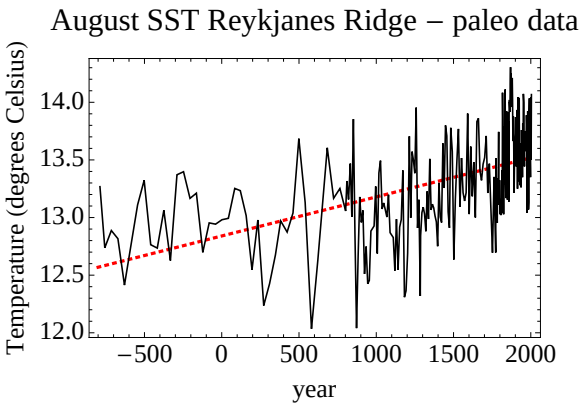

Figure 3.2: *aSST time series Reykjanes Ridge.*
Linear trend estimate: 1 °C/2800 years

Vøring Plateau

Composite core CR 948/2011 from the Norwegian Sea is analyzed in [*Miettinen et al.* (2012), *Berner et al.* (2011)]. It consist of box core JM97-948/2A of length 31 cm, and a giant piston core MD95-2011 of length 17.49 m. Temporal resolution for the composite core is appr. 4 years between 1900-1995, and 3-25 years for the remaining part. Figure 3.3 show the time series with a linear trend of 0.3 °C over 2800 years.

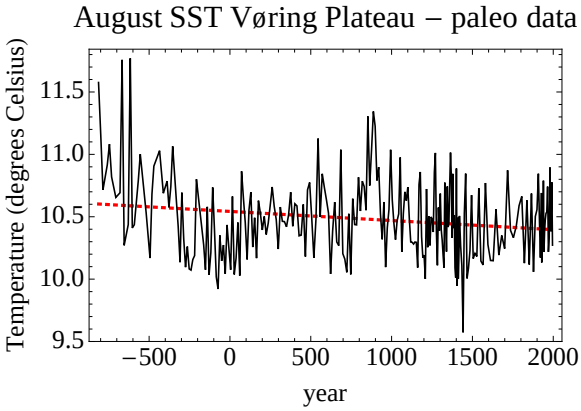

Figure 3.3: *aSST time series Vøring Plateau.*
Linear trend estimate: 0.3 °C/2800 years

3.1.2 Northern Hemisphere temperature reconstruction

[*Moberg et al.* (2005)] combined high and low resolution proxy series of surface temperature (ST) to produce a Northern Hemisphere surface temperature reconstruction for year 0-1978 AD. Tree rings were used as high resolution proxies, while corals, ice cores, pollen, foraminifera, diatoms and stalagmites has lower resolution. Linear interpolation was used to set the lower resolution series to a common annual time increment. A wavelet transform technique was applied to the proxy series in order to obtain a timescale-dependent reconstruction. The beginning and end of the time series were padded to avoid boundary effects on the longest timescales; the mean of the first (last) 50 years of the series were used as padding, so that all time series covered year 300 BC-AD 2300. Wavelet filtering was then used to remove the lowest frequencies from high-resolution time series, and the highest frequencies from the low-resolution proxy series. The Mexican Hat wavelet was used for filtering the time series. More information on the wavelet transformation technique is included in sect. 4.4. The reconstructed time series was at last calibrated by adjusting the mean and variance to match the instrumental records from the period 1856-1979.

3.2 Model data

For the objective of this thesis, one needs to use model runs with realistic external forcing. Because sediment core data represent august temperature, the optimal data set is provided with monthly resolution.
NCDC (national climatic data center) data from two ESMs (Earth system models): COSMOS and LOVECLIM were selected, and climate simulations from the HadCM3 model were downloaded from the ESGF database (Earth system grid federation). Data from the models ECHO-G and ESM CLIMBER-3α has been provided on personal request.
An ESM includes higher level biogeochemistry than an atmosphere-ocean coupled model, by allowing global circulation models (GCMs) to interact with models for

continental ice sheets and the biosphere.
All model data are available in NETCDF format. Simulated SST values are stored as gridded data, i.e. data from the regions of interest must be extracted specifically. Included in most models is a land-sea-mask, which is a matrix where each data point is marked as either land or ocean, or percentage of land.

LOVECLIM model and experiment

The Earth system model LOVECLIM version 1.2 is of intermediate complexity [*Goosse et al.* (2010]. It contains a quasi-geostrophic model for the atmosphere, coupled to an OGCM (ocean GCM). The OGCM is again coupled to a thermodynamic sea-ice model, and the atmosphere and sea-ice-ocean models are connected to a terrestrial biosphere model, an ocean carbon cycle model and an ice sheet model. Data from one experiment with this model is available; "LOVECLIM Climate Model Simulation Constrained by Mann et al. 2009 Reconstruction".[*Goosse et al.* (2010)]. In this experiment, simulations are constrained by the mean surface temperature reconstruction of [*Mann et al.* (2009)]. External forcing includes TSI (total solar irradiance), volcanic eruptions, land cover changes, orbital forcing, greenhouse gases and aerosols. The model output available at NCDC has an annual resolution, and it covers the time period of 501-2000 AD. The SST data have a spatial resolution of 64 x 32 cells, 5.625 x 5.625 degrees each.

CLIMBER-3α model and experiment.

The CLIMBER-3α ESM is a model of intermediate complexity, [*Montoya et al.* (2005), *Mengel et al.* (2012)]. The OGCM is coupled to a statistic-dynamical model for the atmosphere, and models for vegetation and continental ice sheets. External forcing include TSI, volcanoes, anthropogenic aerosols and greenhouse gases, [*Schleussner & Feulner* (2012)]. Annual SST values for the North Atlantic region are available for the time period 1030-1988 AD, with a spatial resolution of 3.75 x 3.75 degrees.

COSMOS model and experiments

The COSMOS ESM consist of GCMs for the atmosphere and the ocean, [*Jungclaus et al.* (2010)]. They are coupled to a sea ice model, an ocean biogeochemistry module and a terrestrial biosphere model. The surface temperature data are available as monthly means. The spatial resolution of the SST values is 96 x 48 grid cells, where each cell is 3.75 x 3.75 degrees. The available set of experiments is referred to as "Ensemble Simulation of the Last Millenium using the Comprehensive COSMOS Earth System Model". It contains global gridded 2 m air temperature, with a monthly resolution, covering the period 800-2006 AD. External forcing used in the forced simulations include TSI, volcanoes, orbital forcing, greenhouse gases and land use change. A group of model experiments performed with the same set of external forcing, but different initial conditions, is called an ensemble. For the COSMOS model, two ensembles of simulations are available. They are produced using different TSI datasets, and contain five and two ensemble members, respectively. An unforced 3100-year control run is also used here in the comparative LRM study.

ECHO-G model and experiment

ECHO-G version 4 consist of GCMs for the ocean/sea ice and the atmosphere. This model is not of ESM type since it includes the ocean and atmosphere modules only. The spatial resolution of SST values is 96x48 cells, 3.75 x 3.75 degrees each. External forcing include volcanoes, solar irradiance and greenhouse gases. Two experiments; Erik1 and Erik2 are used here, both covering the period 1000-1990 AD. Cooler initial conditions separates Erik2 from Erik1. [*Gonzàlez-Rouco et al.* (2003), *von Storch et al.* (2004), *Gonzàlez-Rouco et al.* (2006)].

HadCM3 model and experiment.

The Hadley Centre coupled model 3 has SST values with a spatial resolution of 144 x 288 grid cells, each 1.25x1.25 degrees. It is an AOGCM, but like ECHO-G it is not an ESM, [*Gordon et al.* (2000)]. Monthly mean values are available from one experiment, where external forcing is constant. [*Collins et al.* (2001)].

3.2.1 Model data manipulation

The modeled SST data form a three dimensional (3D) matrix of the longitude, latitude and time. To visualize the spatial distribution, the 3D matrix must be reduced to a 2D format, (eg. latitude and longitude). This can be done by choosing one particular month (COSMOS, ECHO-G, HadCM3) or year (LOVECLIM, CLIMBER). Figure 3.4 displays the temperature distribution for August year 800, COSMOS model, with the landmask edges highlighted in black.

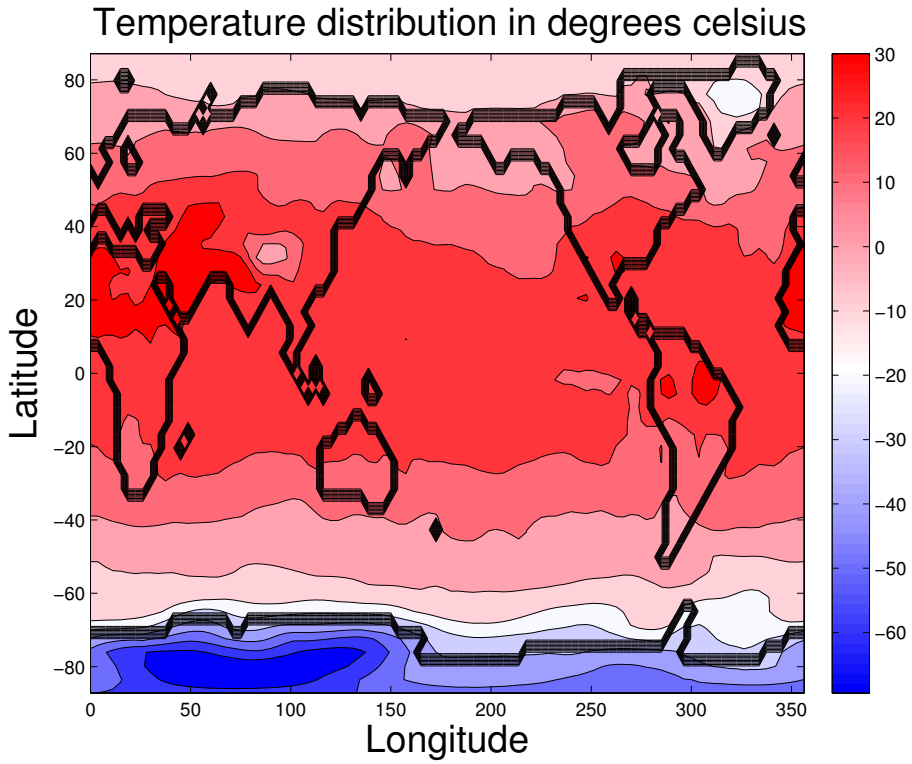

Figure 3.4: *Spatial distribution of August 2 m temperature for year 800 AD, generated by the COSMOS model*

The next step is to extract the temperature data for the regions of interest - Reykjanes Ridge, Vøring Plateau and the Northern Hemisphere. The models do not necessarily reproduce land areas exactly as they appear in reality, due to spatial resolution and simplifications of the land-sea configuration. Note that the longitu-

dinal variable is defined between [0 360], and not [-180 180] which is more conventional. For the regional data extraction, it is therefore wise to choose coordinates by studying a visualization of the model's land-sea mask, see figure 3.5-3.7. For the two regions, only ocean values are to be analyzed. Latitude-longitude "boxes" are selected from the land-sea mask, and the percentage of land is checked for each grid cell within the boxes. Only cells marked as 100 % ocean are of interest, and the SST values in these cells are studied further. Since the core site at the Vøring Plateau is located close to land, it is necessary to include a larger area to obtain any data points. (Grid cells located close to land are marked as 100% land or some % land, and are therefore not used for further studies) [1]. Two separate "boxes" are needed for this region due to the configuration of the models, (see the location of Norway in figure 3.4).
Figure 3.5-3.7 show the approximate positions of the selected regions within the COSMOS model domain.
The mean temperatures for each selected area are calculated by simple averaging of the data values within the region, and weighting by the area of the grid cells, (see appendix A).

The climate simulations from the models used in this study cover the following periods:

- LOVECLIM: annual mean temperatures years AD 501-2000.
- CLIMBER-3α: annual mean temperature years AD 1030-1988.
- COSMOS full forcing exp.: monthly mean temperatures years AD 800-2006.
- COSMOS unforced exp.: monthly mean temperatures years AD 800-3901.
- ECHO-G: monthly mean temperature years AD 1000-1990.
- HadCM3: monthly mean temperature years AD 850-1850.

For the linear trend proxy to model data intercomparison, August values from the two sediment core locations were used for those models where monthly data were available. Annual means were used for the remainig models.

[1] For all models except HadCM3, which has higher spatial resolution.

For the LRM analysis, the surface temperature data series corresponding to the Reykjanes Ridge location and the entire Northern Hemisphere were extracted from the model outputs. The goal of choosing these two data sets is to compare the LRM properties between regional and Hemispheric temperature time series. The Hemispheric temperature data can be compared with the [*Moberg et al.* (2005)] Northern Hemisphere temperature reconstruction, and the regional SST data from Reykjanes Ridge can be compared with the paleodata from the same location. In this thesis, It is assumed that the regional SST signals from the eastern and western North Atlantic region exhibit similar LRM properties, and this is the reason why only one region is chosen for analysis. Note that monthly data from climate simulations were used wherever possible, the seasonal cycle was however subtracted from the data prior to further analysis.

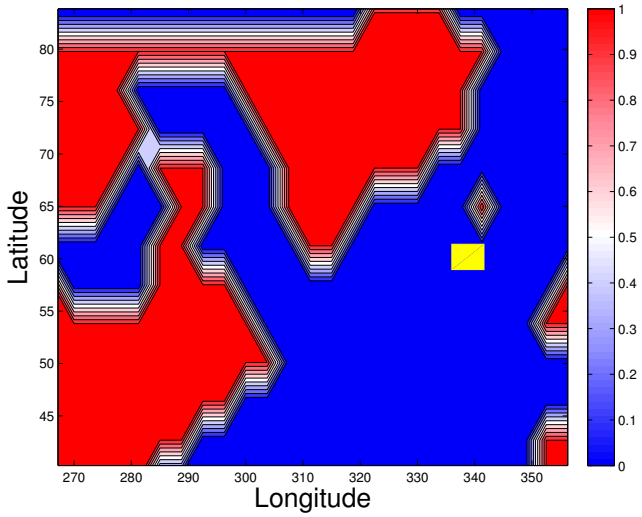

Figure 3.5: *A filled contour plot of a subset of COSMOS' landmask, including the North Atlantic region and surrounding land areas. The figure shows ocean (blue), and land areas (red). The yellow rectangle highlights the selected location for the Reykjanes Ridge*

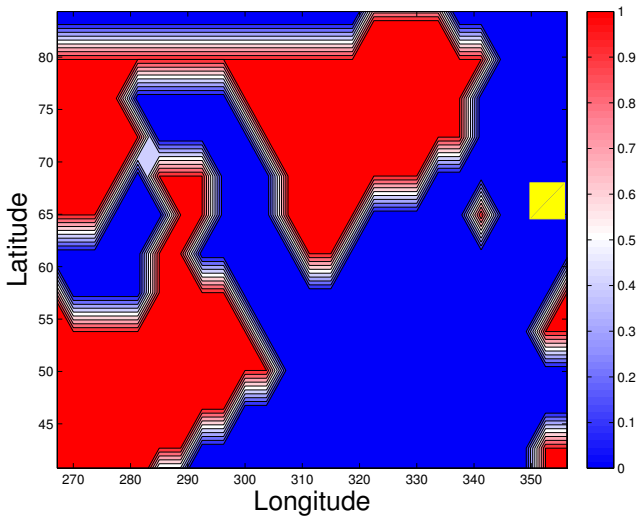

Figure 3.6: *Same map as in figure 3.5. The yellow rectangle highlights the selected location 1 for the Vøring Plateau*

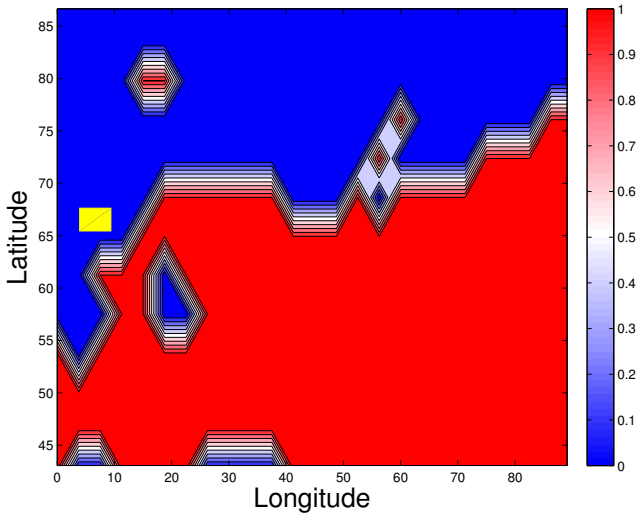

Figure 3.7: *A filled contour plot of another subset of COSMOS' landmask. The yellow rectangle highlights the selected location 2 for the Vøring Plateau*

Chapter 4

Methods of analysis

Analyzing LRM properties in a data set, involves estimating the spectral exponent β or the Hurst exponent. If the data are available with even time steps, such as the [*Moberg et al.* (2005)] Northern Hemisphere temperature reconstruction and simulated time series in this thesis, a multitude of techniques and methods can be applied; e.g. the Fourier transform technique (periodogram), the variogram, and wavelet variance analysis. All methods introduce bias or uncertanties, so using several methods for calculating the β or Hurst exponent is recommended. Both regional and Hemispheric data sets are analyzed, more specifically the data originates from Reykjanes Ridge and the Northern Hemisphere.

The sediment core SST time series are provided with uneven time steps, and the methods above can therefore not be used to detect LRM. Instead, it is assumed that the core data exhibit LRM on time scales up to a few centuries, and that the SST values can be represented as an fGn drawn from a multivariate normal distribution with mean μ, standard deviation σ and Hurst exponent H. Using the fGn hypothesis, the maximum likelihood estimation (MLE) method can be applied to estimate the parameters of the statistical model. H is estimated by this method, and in combination with a numerical Monte Carlo study, the uncertanties are also quantified.

To estimate linear trends in model and paleo data, linear regression analysis is

used.

4.1 Linear regression

[*Miettinen et al.* (2012)] applied linear regression analysis to the time series of reconstructed August SST from Reykjanes Ridge (Rapid21-COM) and the Vøring Plateau (CR-948/2011), in order to infer about the general climate tendencies at the core site locations during the time periods covered by the data. Temperature (Y) is plotted versus time (X), and a straight line is fitted to the data points. The slope of the fitted straight line give indications if there is a trend for the temperature timeseries.

Significance testing using a white noise hypothesis
Statistical significance of the linear trend is assessed with respect to the null hypothesis formulated for the data series under consideration. A white noise statistical model treats the paleo SST values Y as a series of independent samples drawn from an unknown Gaussian distribution. Trend significance is tested by a standard F-test, with the null hypothesis that there is no trend in the data. Such a test may also be applied to a multiple regression model, and the number of independent variables (denoted k) must therefore be specified. In this test, k=1. The F-distribution is associated with k and [n-(k+1)] degrees of freedom, where n is the number of data points, [*Devore & Peck* (1990)].

The F-test:

Test statistic

$$F = \frac{R^2/k}{(1 - R^2)/([n - (k + 1)]}$$

where R^2 is the coefficient of determination, interpreted as the proportion of variation in observed Y values that is explained by the fitted model.

Inserting k=1 yields 1 and n-2 degrees of freedom:

$$F = \frac{R^2}{(1 - R^2)/(n - 2)}$$

The null hypothesis of no trend in the data is rejected if $F > F_{\text{critical}}$.

$$F_{\text{critical}} = (CDF_F)_{\alpha}^{-1}(1, n - 2)$$

where CDF_F is the F cumulative distribution fiunction. The significance level α is set to 0.95.

4.2 Detrending

For the LRM study in this thesis, the hypothesis for all SST time series is that the records can be represented by a stochastic process with power-law scaling (an fGn or fBm). To make the SST records more similar to such stochastic processes, it is desirable to remove linear trends and strong quasi-periodic oscillatory modes. Removal of such features can be performed by fitting a polynomial of order n to parts or to the entire original record. The detrended record is then constructed by the residual values between the original record and the fitted trend. In practice, isolating the stochastic part of a climate record is difficult. Most climate records in this thesis contain internal quasi-periodic oscillations and trends, caused by natural and anthropogenic forcing. Finding the optimal polynomial order is often difficult. Too high order leads to the possibility of incorrectly removing part of the fGn noise while detrending. For the fGn statistical model, there is an intuitive way to check if removal of a trend also removes part of the noise. Look at the periodogram in figure 4.1, respresenting an arbitrarily chosen SST record:

The periodogram of the residual detrended record shows decreased power for the lowest frequencies, which destroys the power-law scaling. Hence, if the climate record is modeled as a trend +fGn, then, it is not appropriate to clarify the 7.th order polynomial as a trend. As a rule of thumb, the polynomial order for the trend should be chosen to give the best power-law scaling in the periodogram of the residual for low frequencies. In the following, a clear linear trend is removed

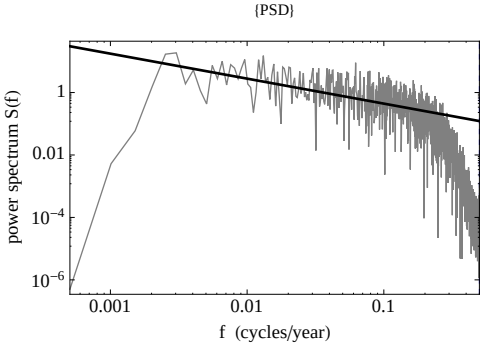

Figure 4.1: *Periodogram of a residual SST record, after removal of 7.th order polynomial trend.*

from the CLIMBER-3α modeled time series. Analysis is then performed for the detrended record. Seasonal variations are removed from all time series with monthly data points.

4.3 Periodogram

A sequence $\{y_n\}, n = 1, 2, ...N$, of N real or complex variables, can be examined in the frequency domain by a decomposition into a finite number of harmonic functions. The discrete Fourier transform (DFT) of the time series is given by:

$$Y_m = FT\{y_n\} = \sum_{n=1}^{N} y_n e^{-i2\pi \frac{(m-1)}{N}(n-1)}, \quad m = 1, 2, 3, ..., N \tag{4.1}$$

Where Y_m is associated with frequency: $f_m = \frac{m}{N}$

The power spectral density, $S(f_m)$ of a time series is a measure of the signal variance at frequency f. It can be expressed as:

$$S(f_m) = \lim_{N\to\infty} \left\{ \frac{2|Y_m|^2}{N} \right\}, \qquad m = 1, 2, 3..., \frac{N}{2} \tag{4.2}$$

When we use $2|Y_m|^2/N$ as an estimate of $S(f_m)$, it is referred to as the periodogram.

For LRM processes, the PSD has a power-law dependence on frequency:

$$S(f_m) \sim {f_m}^{-\beta},$$

Taking the logarithm on each side yields:

$$\log S(f_m) \propto -\beta \log f_m$$

The plot of $\log S(f_m)$ vs $\log f_m$ is the periodogram, where areas with power-law scaling can be identified. A straight line is fitted to this area, providing the estimate of the spectral index β. The Hurst exponent can then be calculated as: $H = (\beta + 1)/2$
In the following periodograms, vertical dashed lines will indicate special features, specified in figure captions. The marked frequency corresponds to a period of $T = 1/f$.

The periodogram-based PSD estimate exhibit an inherent variance that is proportional to the square of the true PSD, [*Zhang et al.* (2005]. The uncertainty of the method is however not critical for this analysis, as the main objective is to assess the scaling properties of the power spectrum and not power in one particular frequency.

4.4 Wavelet Variance Analysis

The wavelet transformation (WT) allows both spatial and frequency variations to be detected in a signal. The WT is essentially a bandpass filter of uniform shape and varying location and width:

$$g\left(\frac{t' - t}{a}\right)$$

which is passed over a time series f(t'), [*Malamud & Turcotte* (1998)]. The filter width is increased by powers of two, and a is a scaling parameter.
The generalized form of the Wavelet transform is given by:

$$W(t, a) = \frac{1}{a^{\frac{1}{2}}} \int_{-\infty}^{\infty} g\left(\frac{t' - t}{a}\right) f(t')\, dt' \tag{4.3}$$

Different Wavelet basis functions exist, and are represented by g(t'). The following must be satisfied:

$$\int_{-\infty}^{\infty} g(t')\, dt' = 0\ ,$$

The "Mexican hat" wavelet basis function is the negative of the second derivative of the Gaussian distribution, and is used in this thesis:

$$g(t') = \left(\frac{1}{2\pi}\right)^{1/2} (1 - t'^2)\, e^{-\frac{1}{2}t'^2} \tag{4.4}$$

Inserting eq. 4.4 into eq. 4.3 yields:

$$W(t, a) = \left(\frac{1}{2a\pi}\right)^{\frac{1}{2}} \int_{-\infty}^{\infty} \left[1 - \left(\frac{t' - t}{a}\right)^2\right] e^{-\frac{1}{2}\left(\frac{t'-t}{a}\right)^2} f(t')\, dt' \tag{4.5}$$

The wavelet coeffients are computed numerically. and then the variances of the wavelet coefficients are estimated:

$$V_w = \frac{1}{N} \sum_{t=1}^{N} |W(t, a)|^2 \tag{4.6}$$

Note that the Fourier period τ is defined as:

$$\tau = \frac{2\pi a}{\sqrt{m + \frac{1}{2}}}$$

For the Mexican hat, m=2 and $\tau \approx 4a$, [*Torrence & Compo* (1998)].

For fGns or fBms, the wavelet variance has the following property, [*Malamud & Turcotte* (1998)]:

$$V_w \sim \tau^{\beta}$$

because of this power-law dependence, β can be estimated by plotting log V_w versus log τ. If there is a range of time scales τ where a straight line can be fitted, do so and find the β value as the slope of the line.

Using the Mexican hat wavelet basis for estimating wavelet variances is efficient, because linear trends are removed. Quasi-periodic oscillations on the other hand, are not eliminated by the second derivative of the Gaussian distribution. A higher derivative can be chosen as the wavelet basis, but other biases are then introduced. Oscillations create artifacts in form of oscillatory features in the (Mexican-hat basis) wavelet variance plots, in the same manner as boundary effects. For a given time scale a, the wavelet coefficient W(t,a) is only correctly estimated for t $\in$ (4a, N-4a), hence unless V_w is estimated only from this interval, there will be biases in V_w for the larger time scales. This effect is particularly strong in presence of a strong trend. If we compute V_w only from the interval (4a, N-4a), we get poor statistics for a $\sim$ N, so I have used the wavelet variance only for scales up to a=N/10.

4.5 The variogram

The variogram γ_k of a time series y_n, n=1,2,3....,N is given by, [*Malamud & Turcotte* (1998)]:

$$\gamma_k = \frac{1}{N-k}\sum_{n=1}^{N-k}(y_{n+k} - y_n)^2 \tag{4.7}$$

where k is the time lag between two values. For a stationary time series x_n, the cumulative sum is formed and used in eq. 4.7:

$$y_n = \sum_{i=1}^{n} x_n$$

For a nonstationary process y_n, γ_k is computed directly from the time series.

From [*Rypdal et al.* (2013)], we find that:

$$\gamma_k \propto k^{2H}$$

Taking the logarithm on each side yields:

$$\log \gamma_k \propto 2H \log k$$

The log-log plot of the variogram is only considered for time scales up to N/10 for the same reasons as for the wavelet variance. From the plot of log γ_k versus log k, a straight line is fitted to linear parts of the curve. The slope of the line give the value of the Hurst exponent directly for a stationary process. For nonstationary processes, H=slope+1.

4.6 Maximum likelihood estimation

Given a data set and a statistical model, MLE provides estimates of the model's parameters. For the study in this thesis, the known values of temperature and time from the uneven sampled paleo data will be assumed to stem from a multivariate normal distribution with LRM (fGn statistical model). H is estimated by MLE from this hypothesis. To verify that the fGn is a suitable model for the paleo climate data, a quantile-quantile plot is used to show how well the data values fit to a normal distribution.

The MLE methodology involves two steps:

(1) The log-likelihood function is formulated:

$$\ln L\,(H|x_i) = \sum_{i=1}^{n} \ln f(x_i|H),$$

where x_i , i=1, 2 .....n are n random values, drawn from a multivariate normal distribution with σ=1, and autocovariance function, γ_t t=0, 1, ...n-1.

$$\gamma_t = \frac{\sigma^2}{2}(|t+1|^{2H} - 2|t|^{2H} + |t-1|^{2H}),$$

Which is the ACF for an fGn with Hurst exponent H, [*Vivero & Health* (2010)], and covariance matrix: $\Gamma_n = (\gamma_{i-j})$. The log-likelihood function can be computed from the covariance matrix, [*McLeod et al.* (2007)].

(2) The ML estimate of H is the value that maximizes the log-likelihood function, when the observed time series is inserted for $\{x_i\}$;

$$\widehat{H} = \text{argmax}[\ln L(H|x_i)],$$

The uncertainty of the ML estimate is then estimated by a Monte Carlo study: 50 realizations of fGns with Hurst exponent $\widehat{H}$ are generated and used as inputs in $L(\widehat{H}, x_i)$. For each realization, a new value $\widehat{H}' = \text{argmax}[\ln L(\widehat{H}|x_i)]$ is estimated. The width of the distribution of the 50 $\widehat{H}'$ values estimate the uncertanties.

Significance testing using the LRM hypothesis

By the LRM hypothesis, significance of a linear trend is tested by MLE and a Monte Carlo study. Note that the paleo SST time series are normalized to be comparable to fGns:

$$x_{\text{normal}} = \frac{x - \bar{x}}{\sigma_x}$$

Where $\bar{x}$ is the mean of x, and σ_x is the standard deviation of x. Trend magnitudes are thereby dimensionless in this section.

- 200 realizations of fGns are generated numerically, with the same number of data points as the paleo time series.
- The linear "trend" magnitude in each time series is computed by regression. (This is simply the spurious trend occuring when linear regression is applied to a realization of an fGn)
- The probability distribution of linear trend magnitudes is presented in a histogram.
- The cumulative distribution function (CDF) of the trend magnitudes is presented in a histogram with a 95% significance level marked on the x axis.

- The linear trend magnitude found from linear regression to the paleo data is placed on the x axis, and significance is determed from whether the point lies outside (significant) or inside (insignificant) the marked area.

Chapter 5

Results

5.1 Detection of LRM in Northern Hemisphere temperature reconstruction and modeled time series

SST anomaly time series, periodograms, variogram and wavelet variance analysis for the NH temperature reconstruction by Moberg and model time series are shown below. The SST anomaly time series is the residual when the mean is subtracted from the original record. β values are used to indicate memory properties, where $0 < \beta < 3$ indicate LRM.
For the wavelet variance, periodograms and variograms, the β value is estimated from the fitted straight line.

Results of LRM study for [*Moberg et al.* (2005)] NH temperature reconstruction.

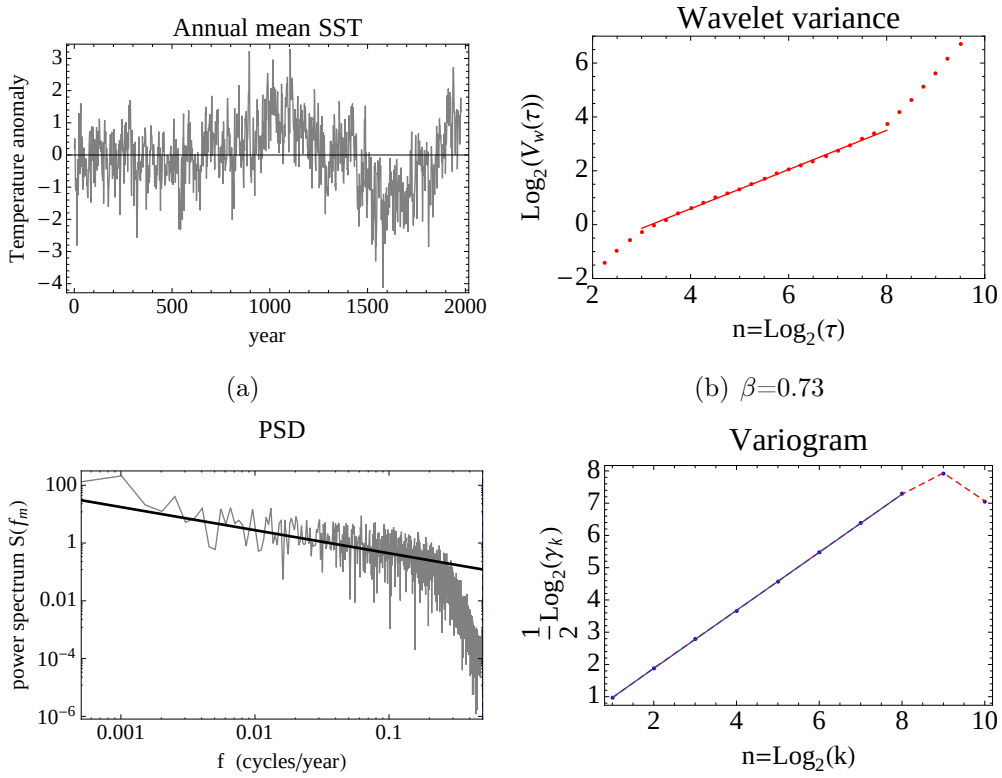

(a) (b) β=0.73

(c) β=0.79 (d) β=0.80

Figure 5.1: *Panel (a): the temperature anomaly record for annual mean values, for the time period 0-1978 AD. (b): the wavelet variance of the anomaly is represented by red dots, and the solid line is fitted between n=3:8. The estimated β value is presented below the subfigure. (c): the periodogram with fitted line slope β. The deficiency in power at the highest frequencies is an artifact caused by smoothing of the record. (d): the variogram is calculated from the cumulative sum of the ST anomaly record. β is estimated indirectly from a linear fit between n=1:8, β=2H-1, when H is the slope of the fitted line.*

The temperature reconstruction exhibits LRM on time scales up to at least a few centuries, with $\beta \approx 0.75$. On the shortest time scales, smoothing of the

reconstructed data potentially introduces bias to the estimates of the periodogram and the wavelet variance. Boundary effects and the oscillation of period of about 1000 years create a larger slope for time scales higher than 260 years for the wavelet variance. According to [*Rypdal & Rypdal* (2013)], this oscillation is caused by a combination of volcanic and solar forcing.

Results of LOVECLIM LRM study - Reykjanes Ridge

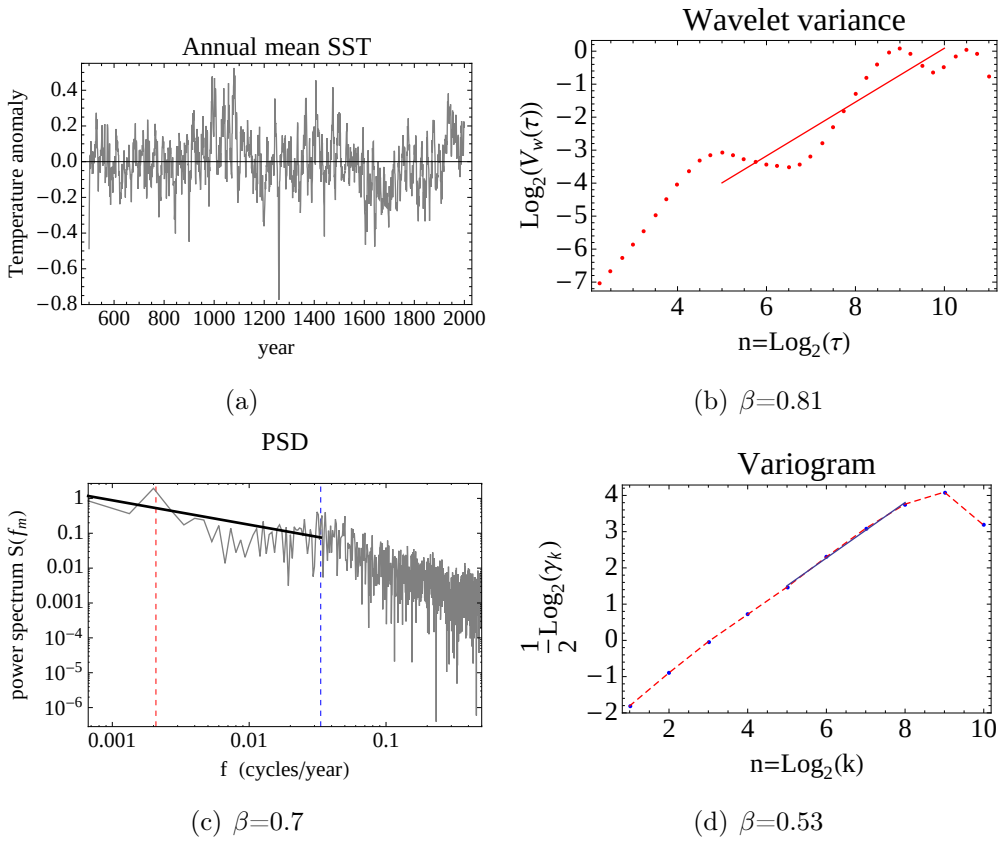

(a) (b) β=0.81

(c) β=0.7 (d) β=0.53

Figure 5.2: *Panel (a): temperature anomaly record (annual mean values) for the time period 501-2000 AD. Variability in a broad range of frequencies is observed. (b): the wavelet variance with fitted line between n=5:10. Quasi-periodic oscillations in the SST time series creates artifacts in the wavelet variance plot. (c): The periodogram with fitted line for time scales larger than 30 years. The dashed blue line marks the change in scaling at this time scale. The dashed red line marks a local power maximum at the time scale of ca. 500 years. (d): the variogram is estimated from the cumulative sum of the SST anomaly record, and the line is fitted between n=5:8.*

Detrending of the 500 year oscillation is not performed in order to preserve the stochastic part of the record. LRM is detected on the longest time scales.

Results for LOVECLIM LRM study - Northern Hemisphere

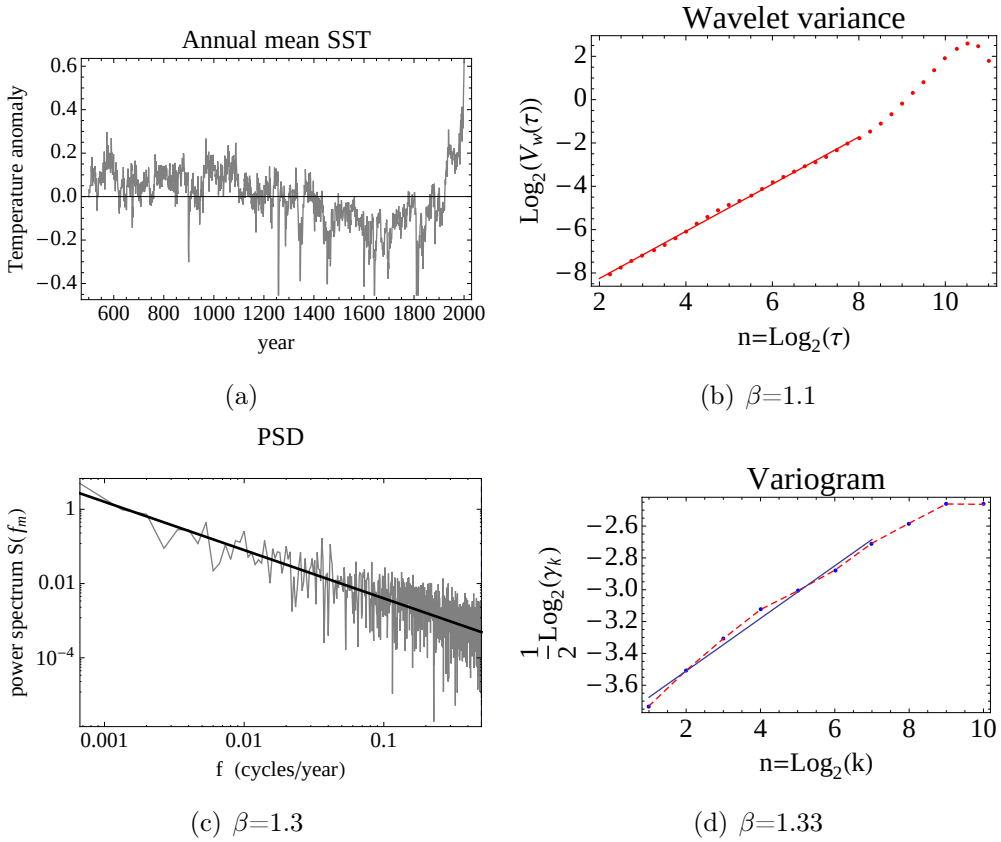

(a) (b) β=1.1

(c) β=1.3 (d) β=1.33

Figure 5.3: *Panel (a): the Hemispheric time series is similar to the Moberg reconstruction. The positive trend seen for the last 150 years, is generally associated with anthropogenically induced global warming. (b): the wavelet variance is smooth up to n=8, where the millenium oscillation and boundary effects create artifacts on the longest time scales. The line is fitted between n=2:8. (c): the periodogram follows a power law on all time scales. (d): the variogram is calculated directly from the ST anomaly record. The line is fitted between n=1:7*

The record exhibit LRM up to a few centuries. β is slightly higher than for the Moberg reconstructed SST record, meaning it has stronger persistence.

Results for CLIMBER-3α LRM study - Reykjanes Ridge

Since the available data from this simulation only cover the North Atlantic Ocean, analysis is only performed for Reykjanes Ridge.

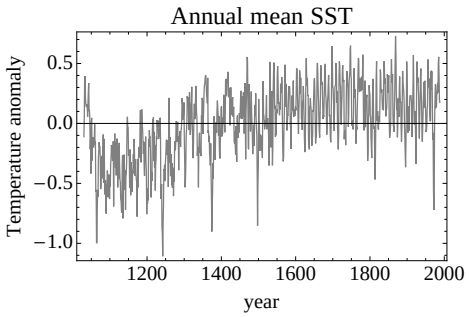

(a) Original signal

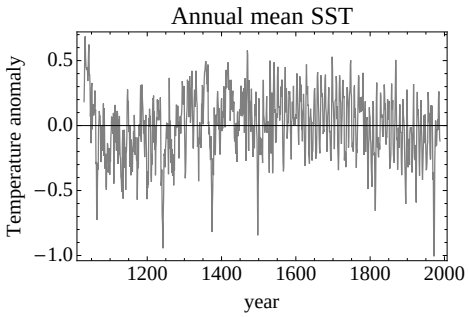

(b) Detrended signal

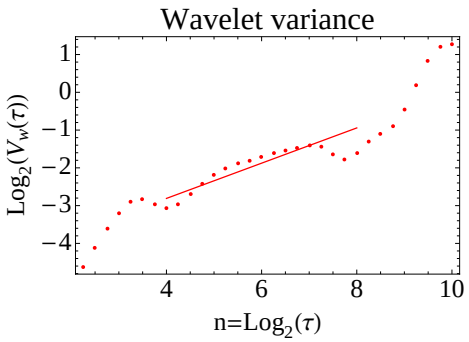

(c) β=0.47

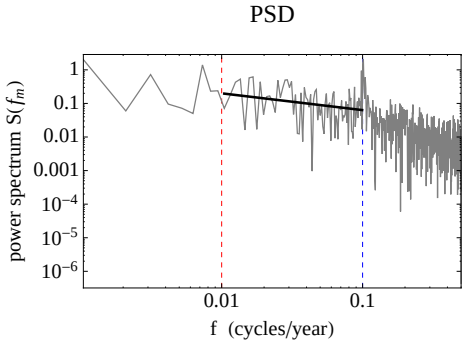

(d) β=0.5

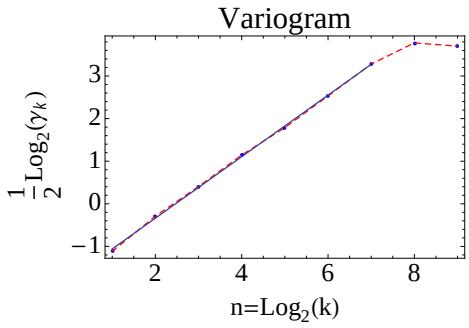

(e) β=0.46

Figure 5.4

Figure 5.4: *Panel (a): the temperature anomaly record (annual mean values) for the time period 1030-1988 AD. A positive linear trend of 0.58°C/958 years is observed, as well as oscillations. (b): detrended signal when the linear trend is removed. (c): wavelet variance for the detrended signal. The line is fitted between n=4:8. (d): the periodogram show a frequency peak at about 10 years (dashed blue line). A pronounced change in the continuum is seen at this point. A similar feature is observed again at the time scale of 100 years (dashed red line). (e): the variogram is calculated from the cumulative sum of the SST anomaly record.β is estimated for the scales n=1:7.*

The frequency peak observed in the periodogram at time scales around 10 years, is possibly the model representation of the NAO (North Atlantic Oscillation). The NAO has a frequency $\sim$ 10 years, and is a quasi-periodic mode of climate variability in the North Atlantic Ocean. Some GCMs are able to represent the variability associated with this mode, [*IPCC* (2007)].
Both the wavelet variance analysis, periodogram and the variogram estimate $\beta \sim$ 0.5 on the chosen time scales. This indicate persistence, and LRM up to a few centuries.

Results for COSMOS full forcing LRM study - Reykjanes Ridge

LRM properties for one full forcing experiment for the COSMOS model are analyzed, and presented in figure 5.5 .

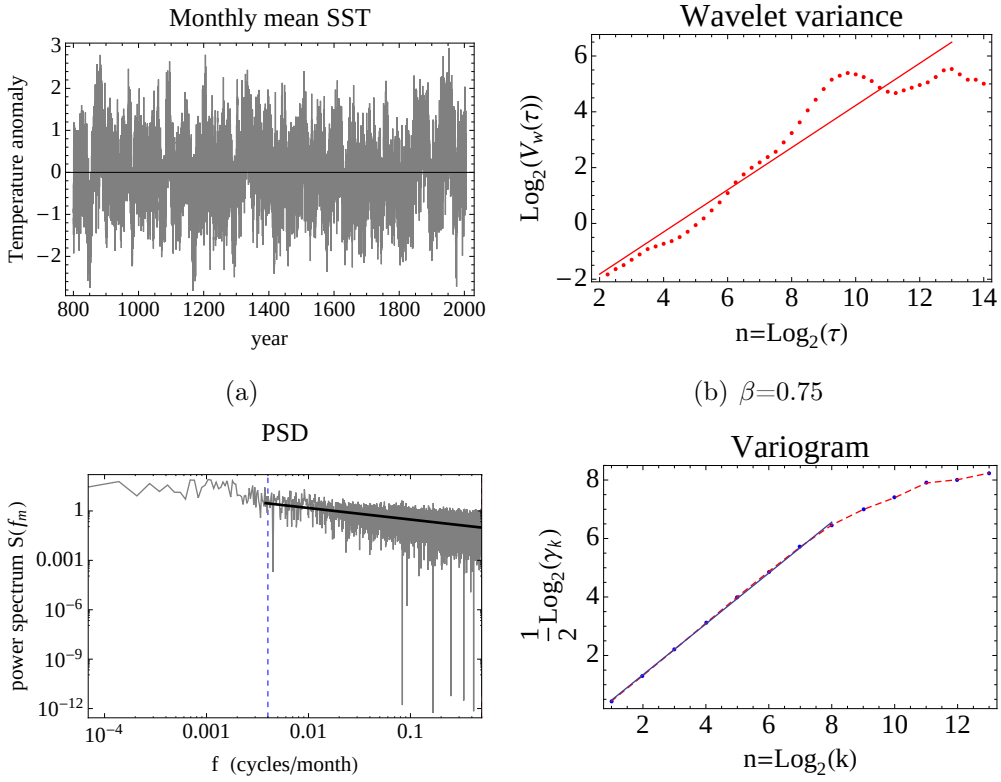

(a) (b) β=0.75

(c) β=0.7 (d) β=0.74

Figure 5.5: *Panel (a): temperature anomaly record (monthly mean values) for the time period 800-2006 AD. (b): the wavelet variance with fitted line between n=2:13. (c): The dashed blue line in the periodogram marks a change in the slope at 250 months=22 years. (d): the variogram is estimated from the cumulative sum of the SST anomaly values. It changes slope at* 2^8 *months=21 years.*

LRM is detected on time scales up to a few decades. The signal then evolves into a white noise-like process.

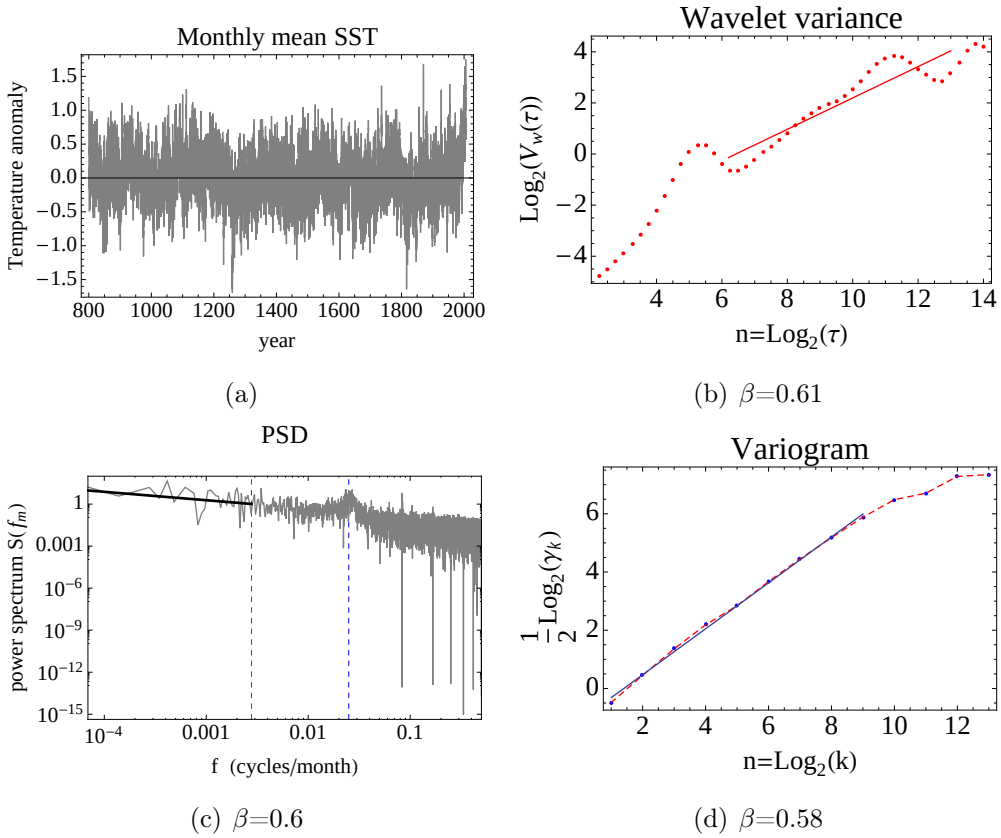

Figure 5.6: *Panel (a): temperature anomaly record. (b): Wavelet variance, with fitted line between n=6.2:13. (c): the dashed blue line in the periodogram marks a frequency peak at appr. 3 years. The dashed red line marks a change in slope at appr. 30 years. (d): the variogram is calculated from the cumulative sum of the ST anomaly values. the line is fitted between n=1:9*

the curve seen at 2^5 months=3 years in the wavelet variance and periodogram, is possibly the model representation of the climatic oscillation ENSO (El Niño Southern Ocillation, frequency 2-7 years). ENSO is a quasi-periodic mode of climate variability in the tropical Pacific with a global imprint on surface temperatures. [*IPCC* (2007)] claim that GCMs indeed simulate variability similar to ENSO. The record exhibit LRM up to at least a few centuries.

Results for COSMOS unforced experiment LRM study - Reykjanes Ridge

An unforced experiment is intended to reveal the possible drifts in the model, as well as its intrinsic variability not related to external forcing factors.

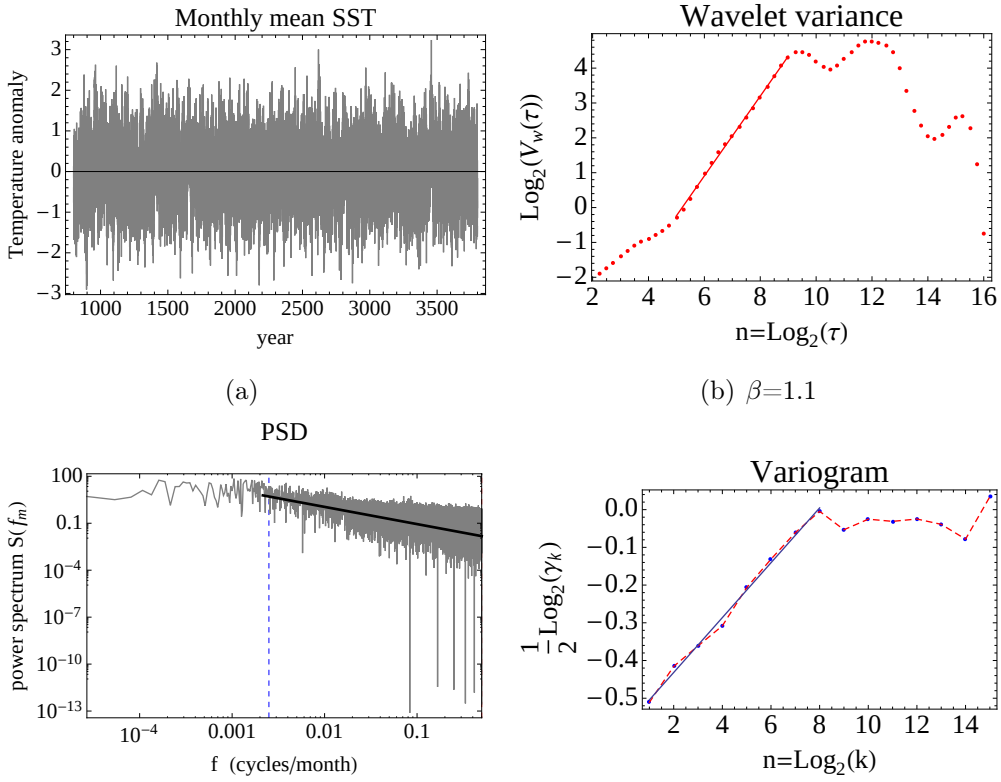

(a) (b) β=1.1

(c) β=1.1 (d) β=1.14

Figure 5.7: *Panel (a): temperature anomaly record (monthly mean values) for the time period 800-3901 AD. (b): wavelet variance. The line is fitted between n=5:9. (c): the periodogram changes slope after appr. 30 years (dashed blue line). For shorter time scales, the PSD scales like an fBm. On longer time scales, the spectrum is flat. (d): the variogram is calculated directly from the SST anomaly values, and the line is fitted between n=1:8.*

The record evolves from a persistent fBm-like process into a white noise after a few decades.

Results for COSMOS unforced experiment LRM study - Northern Hemisphere

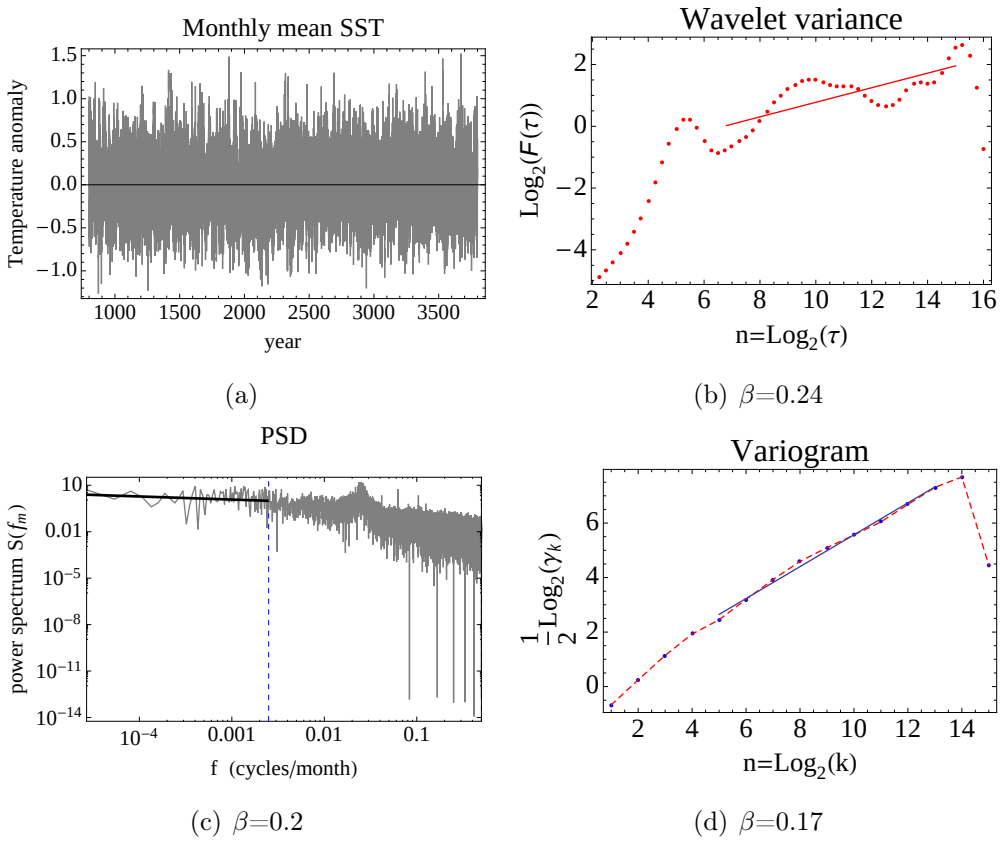

(a) (b) β=0.24

(c) β=0.2 (d) β=0.17

Figure 5.8: *Panel (a): temperature anomaly record. (b): wavelet variance. The line is fitted between n=6.8:15. (c): the periodogram. The PSD flattens after 30 years (dashed blue line). (d): the variogram is estimated from the cumulative sum of the ST anomaly values. The line is fitted between n=5:13.*

The oscillation with a 3-year period is observed from the wavelet variance and the periodogram. The signal is similar to a white noise on time scales longer than 3 years.

Results for ECHO-G LRM study - Reykjanes Ridge

The plots in figure 5.9 represent analysis of ECHO-G Erik1 experiment. Analysis has been performed for Erik2 as well, with the results fairly similar between the two experiments.

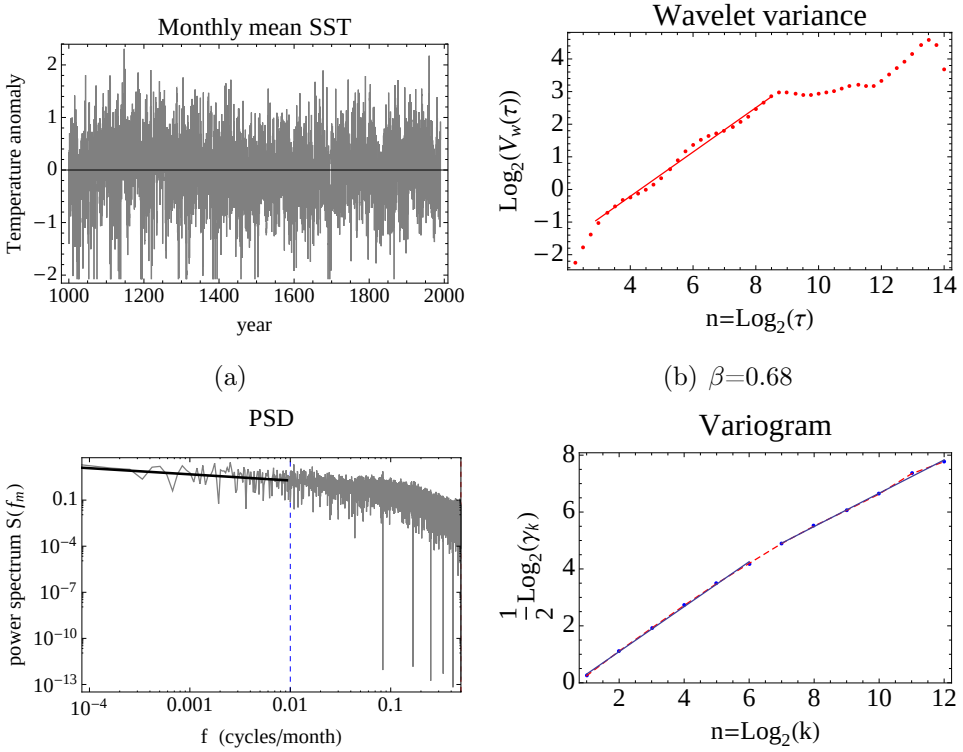

(a) (b) β=0.68

(c) β=0.4 (d) β=0.58, 0.16

Figure 5.9: *Panel (a): temperature anomaly record (monthly mean values) for the time period 1000-1990 AD. (b): the wavelet variance, with fitted line between n=2.9:8.5. (c): the periodogram. The dashed blue line marks a transition at appr. 8 years. (d): the variogram display a break at* 2^6 *months =5.3 years. For longer timescales, the signal is similar to a white noise. The lines are fitted between n=1:6 and n=7:12.*

Note that a power law is not suitable for the highest frequencies of the periodogram.

Results for ECHO-G LRM study - Northern Hemisphere

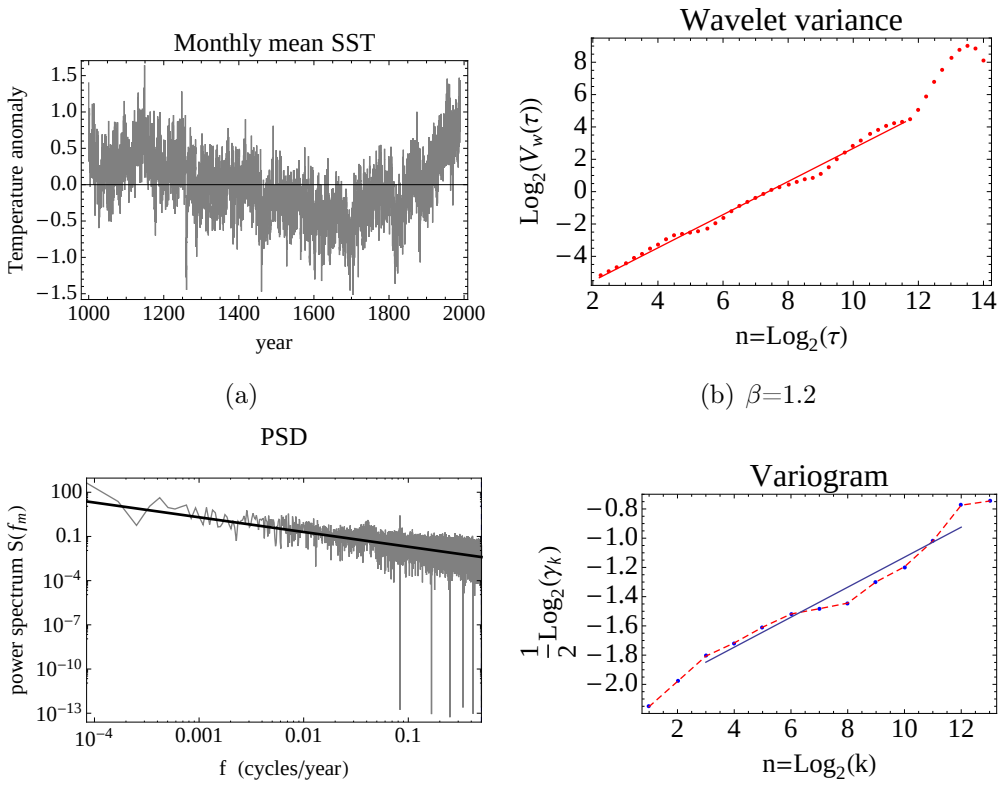

(a) (b) β=1.2

(c) β=1.0 (d) β=1.18

Figure 5.10: *Panel (a): the Hemispheric temperature anomaly record from Erik1 is similar to the Moberg reconstruction. The temperature increase from about 1850 is again generally associated with anthropogenically induced global warming. (b): the wavelet variance. The line is fitted between n=2.2:11.6. (c): the periodogram follows a power law on all time scales. (d): the variogram is calculated directly from the ST anomaly values. The line is fitted between n=3:12.*

The record is persistent, and exhibit LRM up to a few centuries.

Results for HadCM3 LRM study - Reykjanes Ridge

The time series from the HadCM3 model is produced with constant forcing, and note that greenhouse gas concentrations are preindustrial.

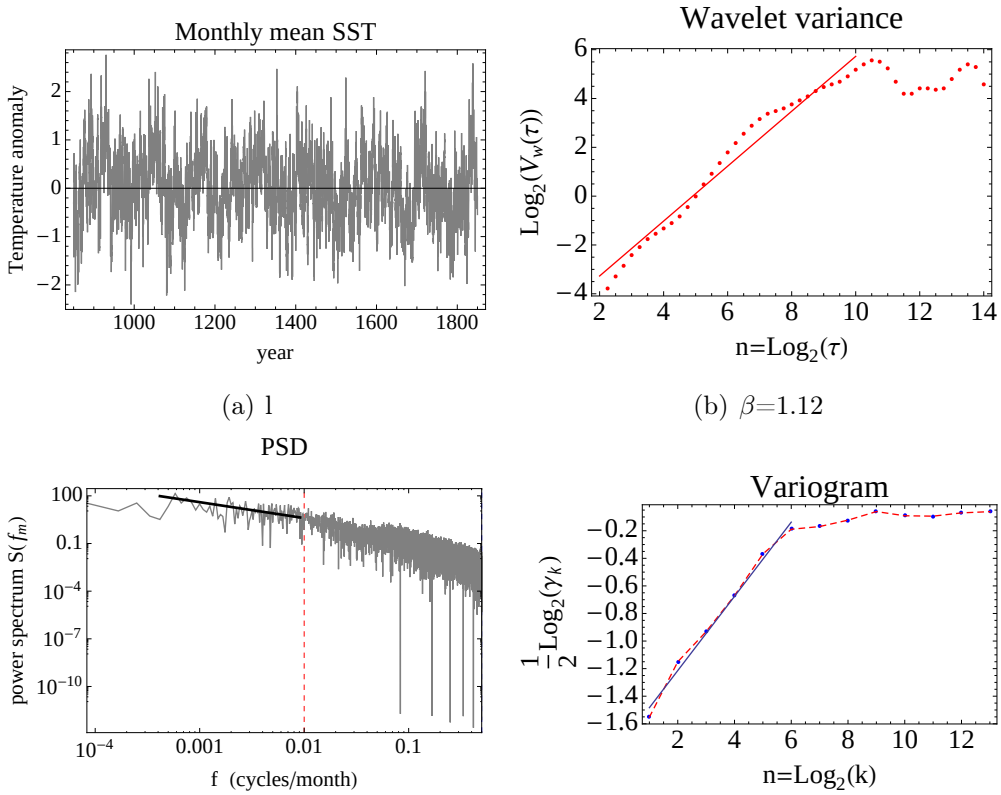

(a) l (b) β=1.12

(c) β=1.0 (d) β=1.54

Figure 5.11: Panel (a): Temperature anomaly record (monthly mean values), for the time period 850-1850 AD. Multiple quasi-periodic oscillations are observed. (b): the wavelet variance. The line is fitted between n=2:10. (c): The periodogram changes slope at time scales from appr. 8 years (dashed red line). (d): The variogram is calculated directly from the SST anomaly values. The line is fitted between n=1:6.

The signal evolves from an fBm with high persistence to a pink noise after a few decades.

Results for HadCM3 LRM study - Northern Hemisphere

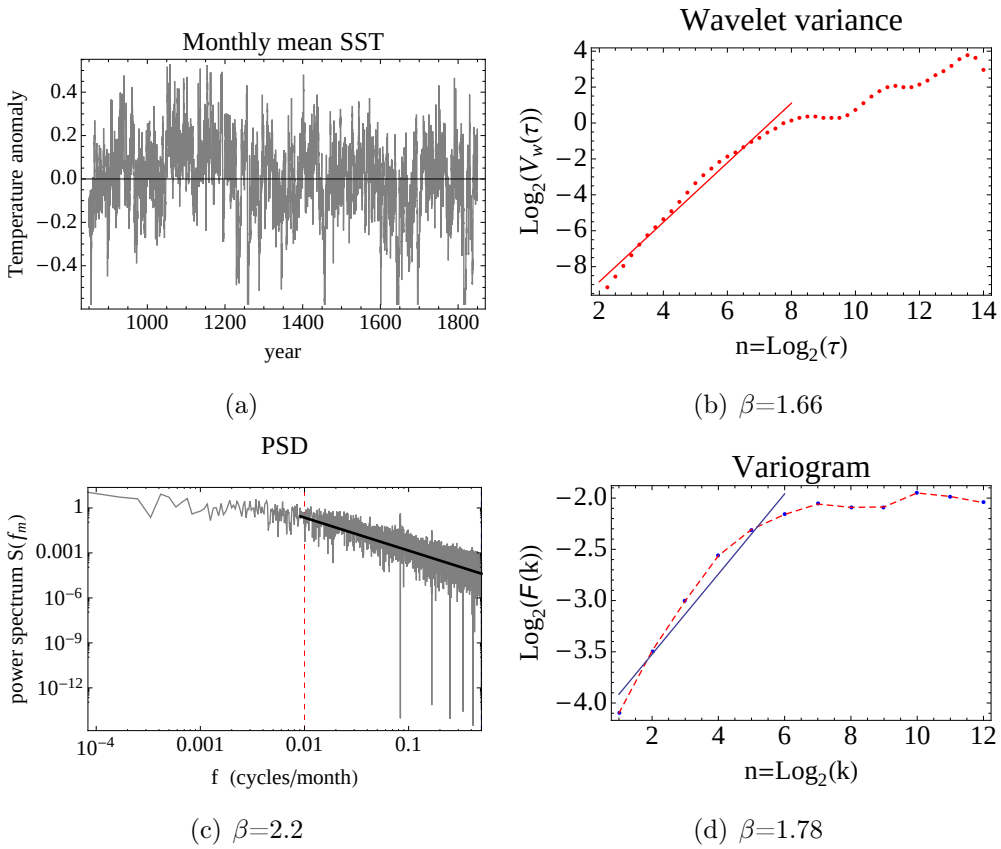

(a) (b) β=1.66

(c) β=2.2 (d) β=1.78

Figure 5.12: *Panel (a): the Hemispheric temperature anomaly SST record. (b): the wavelet variance. The line is fitted between n=2:8. (c): the periodogram changes character after 8 years (dashed red line). (d): the variogram is estimated directly from the ST anomaly values. The line is fitted between n=1:6.*

The record evolves from an fBm to a persistent white noise-like process after a few years. Because β is near 2 at short time scales, the record is similar to an AR(1) process, but the persistence on scales longer than a decade observed in the periodogram and the wavelet variance shows that an fGn is a better model on those scales.

5.2 Linear trend analysis

For the paleoproxy SST data, previously published results are presented in [*Miettinen et al.* (2012)]. The trend estimates are based on a white noise null hypothesis, and represent year 800 BC to 2000 AD. A warming trend of 1 °C is found for the core data from the western subpolar North Atlantic, and a cooling trend of 0.3 °C is found for the eastern part.
In the present study, paleo data are compared with model results. It is therefore necessary to make new trend estimates for the paleo proxy based SST reconstructions, using the time periods that overlap with the time periods represented by the model experiments considered here: LOVECLIM 501-2000 AD, CLIMBER-3α 1030-1988 AD, COSMOS 800-2006 AD, ECHO-G 1000-1990 AD and HadCM3 850-1850 AD.
The time series of the model data include annual or monthly mean values. To make comparison with paleo data more accurate, the analyzed time series are resampled to decadal means. All trends calculated for the model and paleo data are tested by a white noise null hypothesis significance test, referred to as the F-test.

Trends without significance are denoted "not significant", abbreviated NS.

Table 5.1 shows the estimated magnitudes of linear trends in SST temperature for the LOVECLIM model data, year 501-2000 AD, and paleoproxy SST reconstructions for the same time period:

	Reykjanes Ridge °C /1500 y	Vøring Plateau °C /1500 y
Core	+0.93	-0.38
Model	NS	NS

Table 5.1: *Linear trend magnitude - LOVECLIM model and paleoproxy data, year 501-2000 AD*

No significant linear trends observed in model data.

Table 5.2 shows the estimated magnitudes of linear trends in SST temperature for the CLIMBER-3α model data, year 1030-1988 AD, and paleoproxy SST reconstructions for the same time period:

	Reykjanes Ridge °C /958 y	Vøring Plateau °C /958 y
Core	+0.7633	NS
Model	+0.5754	-1.4803

Table 5.2: *Linear trend magnitude - CLIMBER-3α model and paleoproxy data, year 1030-1988 AD*

The model results feature opposite trends in the two areas under consideration. This is in line with the results inferred from the proxy-based reconstruted SST. Figure 5.13 show the spatially distributed linear trend magnitudes for the North Atlantic Ocean.

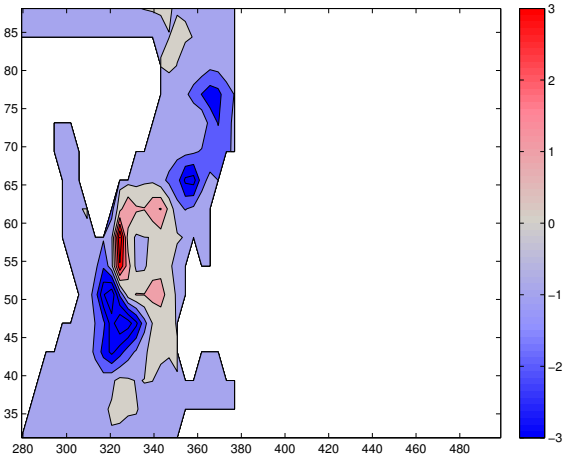

Figure 5.13: *Spatial distribution of changes in North Atlantic annual mean SST in the forced simulation CLIMBER over the time period 1030-1988 AD. White areas surrounding the North Atlantic Ocean (colored), are land masses. The color bar to the right shows the magnitude of SST change.*

Table 5.3 shows the estimated magnitudes of linear trends in SST temperature for the COSMOS full forcing model data, year 800-2006 AD, and paleoproxy SST reconstructions for the same time period:

N=Model ensemble number and member.

	Reykjanes Ridge °C /1206 y	Vøring Plateau °C /1206 y
Core	+0.85	-0.35
N 1.1	NS	-0.33
N 1.2	NS	-0.67
N 1.3	NS	-0.52
N 1.4	NS	-0.78
N 1.5	NS	-0.63
N 2.1	NS	NS
N 2.2	NS	NS

Table 5.3: *Linear trend magnitude - COSMOS full forcing model and paleoproxy data, year 800-2006 AD*

Results from ensemble 1 shows statistically significant cooling in the Vøring Plateau area, similar in magnitude to the cooling inferred from the MD95-2011 SST reconstruction. No significant trend has been detected in the Reykjanes Ridge area.

Table 5.4 shows the estimated magnitudes of linear trends in SST temperature for the ECHO-G model data, year 1000-1990 AD, and paleoproxy SST reconstructions for the same time period:

The ECHO-G time series are the shortest in this study. No significant linear trends are found for the model data.

	Reykjanes Ridge °C /990 y	Vøring Plateau °C /990 y
Core	+0.83	NS
Erik1	NS	NS
Erik2	NS	NS

Table 5.4: *Linear trend magnitude - ECHO-G model and paleoproxy data, year 1000-1990 AD*

Table 5.5 shows the estimated magnitudes of linear trends in SST temperature for the HadCM3 model data, year 850-1850 AD, and paleoproxy SST reconstructions for the same time period:

	Reykjanes Ridge °C /1000 y	Vøring Plateau °C /1000 y
Core	+0.5659	-0.6365
Model	NS	-0.4153

Table 5.5: *Linear trend magnitude - HadCM3 model and paleoproxy data, year 850-1850 AD*

The results from table 5.5 show that a significant linear trend for the model data is found for the Vøring Plateau area, but not Reykjanes Ridge.

5.2.1 Detection of MWP, LIA and antiphasing of features

The MWP and LIA are climate anomalies. [*Miettinen et al.* (2012)] found a warming of the SST in the Vøring Plateau during the medieval warm period (MWP), that ocurred in parallell with cooling at Reykjanes Ridge. The opposite pattern emerged during the little ice age (LIA), suggesting the existence of an SST seesaw between the subpolar North Atlantic and the Norwegian Sea.
For the model time series, the MWP and LIA is detected by studying the plots of

decadal SST. The two features are marked by blue and red rectangles. Significant antiphased features are marked by green rectangles.

Detection of the MWP, LIA and antiphasing of features - LOVECLIM

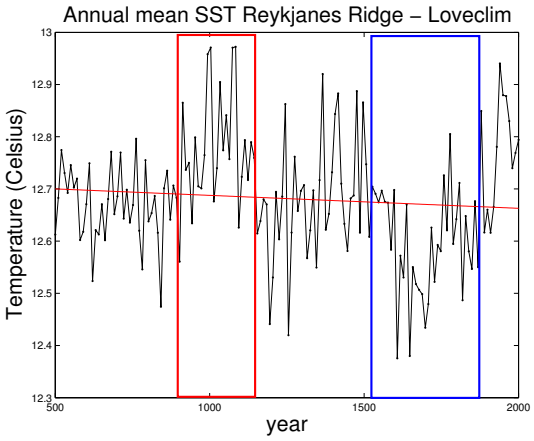

(a) *MWP in red rectangle, LIA in blue*

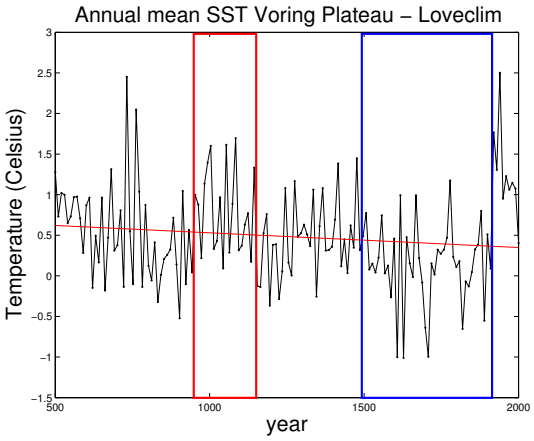

(b) *MWP in red rectangle, LIA in blue*

Figure 5.14: *Regional SST time series for the LOVECLIM simulation, for the time period AD 501-2000.*

The LOVECLIM model does represent the MWP and LIA for the two regions. Local features are mostly in phase.

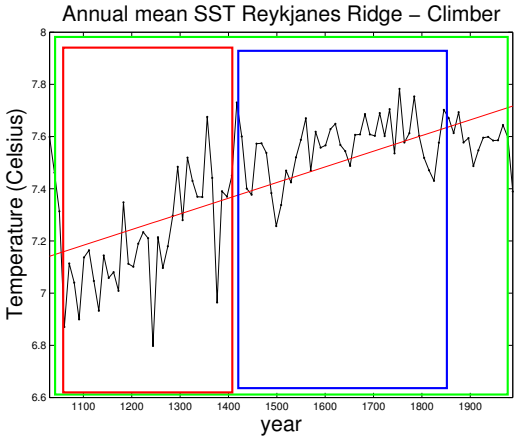

(a) *MWP in red rectangle, LIA in blue, and antiphasing for the entire period marked by green.*

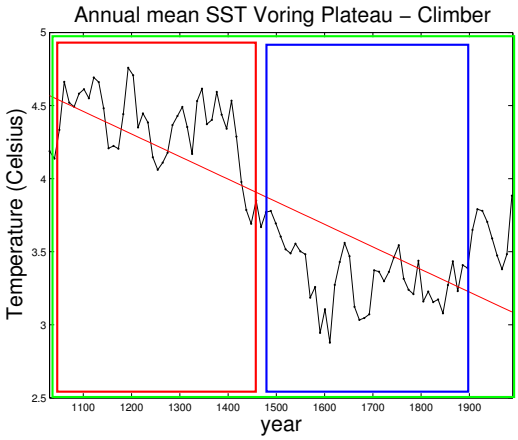

(b) *MWP in red rectangle, LIA in blue, and antiphasing for the entire period marked by green.*

Figure 5.15: *Regional SST time series for the CLIMBER simulation, for the time period AD 1030-1988.*

The CLIMBER-3α model shows diverging trends for the entire period considered. Both the MWP and LIA are visible for both regions, and the SST records from Reykjanes Ridge and Vøring Plateau are in antiphase with each other.

Detection of the MWP, LIA and antiphasing of features - COSMOS ensemble 2 member 1

The plots of decadal mean SST for all COSMOS full forcing experiments have been studied, but only ensemble 2 member 1 in figure 5.16 reproduces the MWP and LIA.

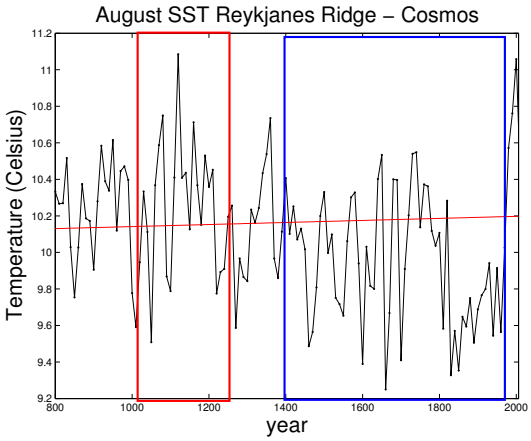

(a) *MWP in red rectangle, LIA in blue*

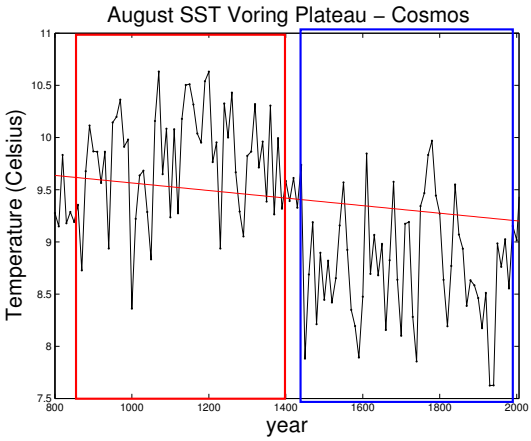

(b) *MWP in red rectangle, LIA in blue*

Figure 5.16

Figure 5.16: *Regional SST time series for COSMOS ensemble 2 member 1, full forcing simulation, for the time period AD 800-2006.*

The COSMOS model reproduce the MWP and LIA only in 1 out of 7 realizations. Only the initial conditions separates the experiments, so the fact that detected features correspond to the MWP and LIA are possibly sheer coincidence. For all other realizations, the temperature is generally stable and does not show significant features. The SST between the eastern and western North Atlantic are nearly coherent on secular time scales in this model, indicating no antiphasing between the regions.

Detection of the MWP, LIA and antiphasing of features - ECHO-G Erik1

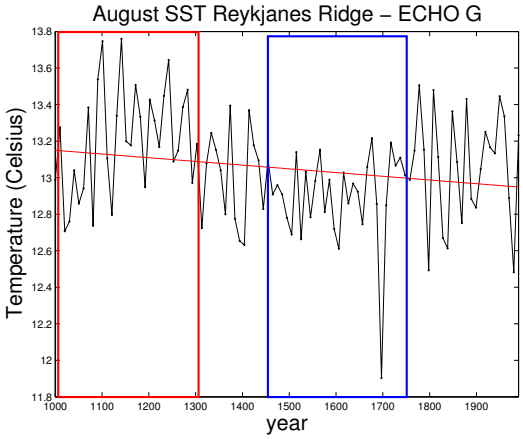

(a) *MWP in red rectangle, LIA in blue*

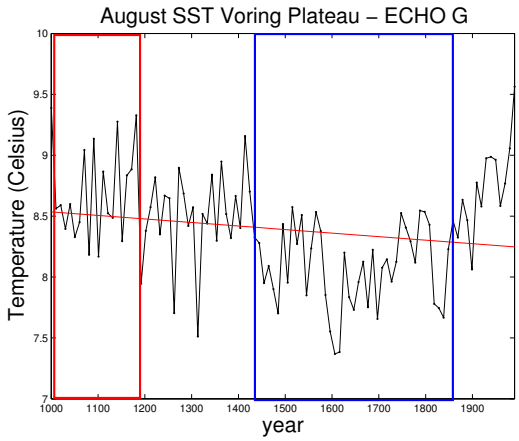

(b) *MWP in red rectangle, LIA in blue*

Figure 5.17: *Regional SST time series for ECHO-G Erik1 simulation, for the time period AD 1000-1990.*

The ECHO-G model, Erik1 simulation of the climate of the past millenium, show that the MWP and LIA are in phase for the two considered regions.

Detection of the MWP, LIA and antiphasing of features - ECHO-G Erik2

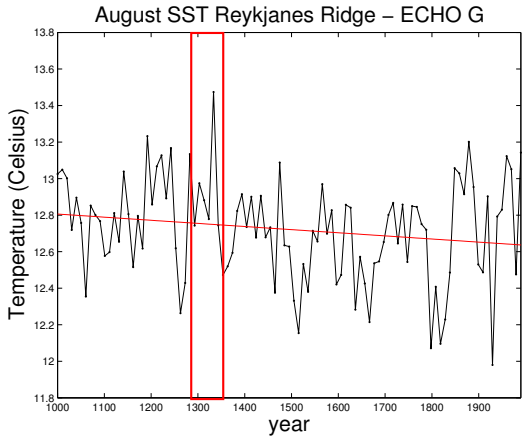

(a) *MWP in red rectangle, LIA in blue*

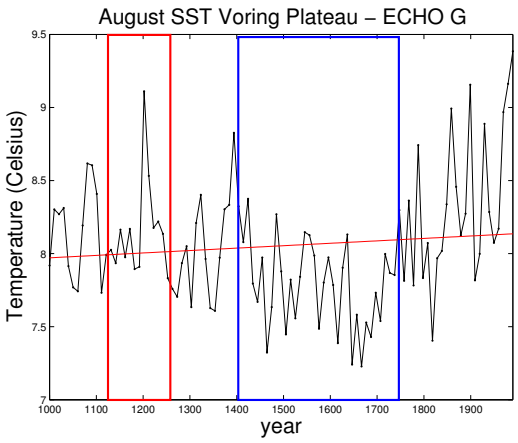

(b) *MWP in red rectangle, LIA in blue*

Figure 5.18: *Regional SST time series for ECHO-G Erik2 simulation, for the time period AD 1000-1990.*

The Erik2 simulation, in contrast to Erik1, shows a less prominent transition from the MWP to the LIA. The onset of the LIA in the mid 15^{th} century is clear for the model data from the Vøring Plateau, but not from the Reykjanes Ridge. The MWP is not lasting in any of the study areas. It is visible only as shorter peaks.

Detection of the MWP, LIA and antiphasing of features - HadCM3

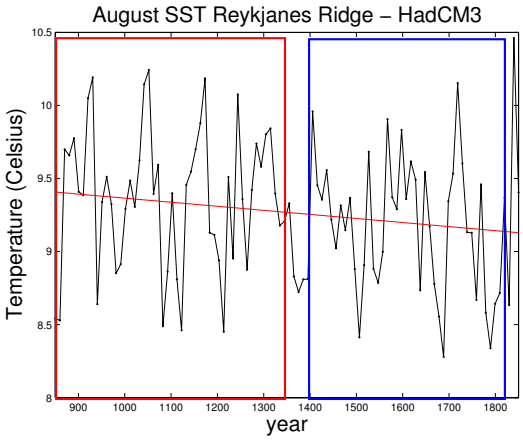

(a) *MWP in red rectangle, LIA in blue*

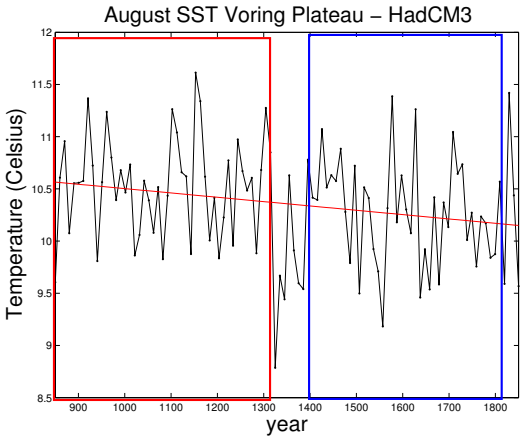

(b) *MWP in red rectangle, LIA in blue*

Figure 5.19: *Regional SST time series for HadCM3 simulation, for the time period AD 850-1850.*

The HadCM3 simulation in figure 5.19 exhibits a cooling trend for the two selected areas. The submillenial scale variability is fairly weak, showing no signs of the pronounced MWP and LIA climate anomalies in any of the two regions considered.

5.3 LRM null hypothesis applied to regional paleo climate data

Analyzing the SST time series using an LRM null hypothesis, implies that the data set under consideration can be represented by an fGn statistical model with mean μ, standard deviation σ and memory exponent H. The MLE method is applied to estimate the Hurst exponent, and a Monte Carlo study is performed to estimate the uncertanties. The significance of the linear trends of the sediment core SST time series are tested by the LRM null hypothesis, by another Monte Carlo study.

5.3.1 Reykjanes Ridge

The QQ-plot (quantile-quantile plot) in figure 5.20 shows that a normal distribution is a good choice for the paleo data:

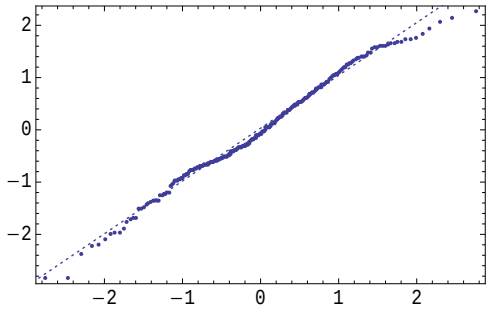

Figure 5.20: *Quantile deviation for Reykjanes Ridge paleo data from a normal distribution*

ML estimate of H for the paleo data: H=0.91, β=0.82.

A Monte Carlo study with 50 realizations of fGns with H=0.91 give the likelihood functions presented in figure 5.21. ML estimates of H for all 50 realizations are presented by their probabilities in figure 5.22.

The standard deviation of the estimates: σ=0.012.

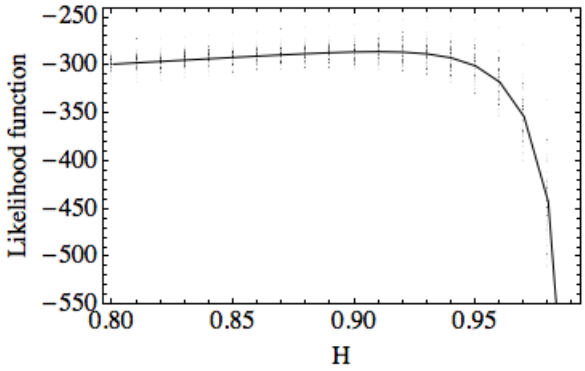

Figure 5.21: *Likelihood functions for H are shown as error bars for the 50 realizations of fGns with prescribed H=0.91. The solid line is the mean likelihood function.*

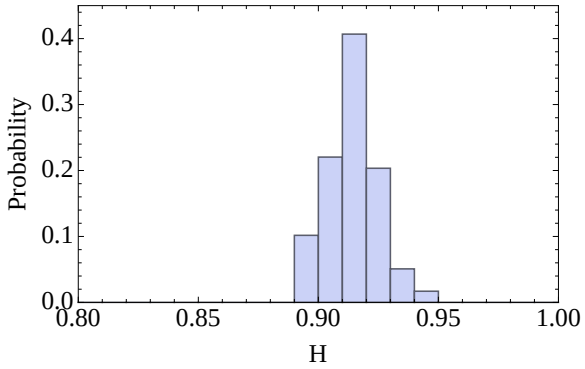

Figure 5.22: *Probability density distribution of H estimates.*

Figure 5.23 show linear trends calcuated from 200 realizations of fGns with the prescribed memory exponent H=0.91. Figure 5.24 show the histogram of the cumulative distribution function of trends.

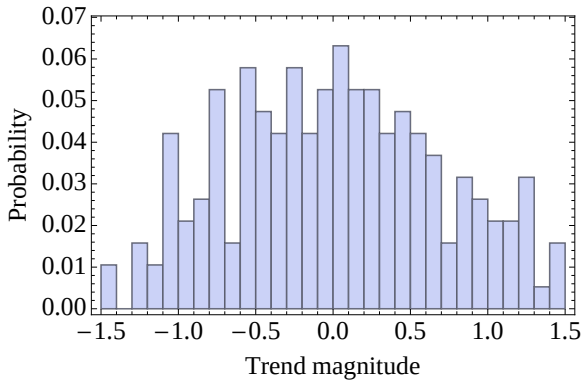

Figure 5.23: *Probability distribution of linear trends calculated from 200 realizations of fGns with H=0.91*

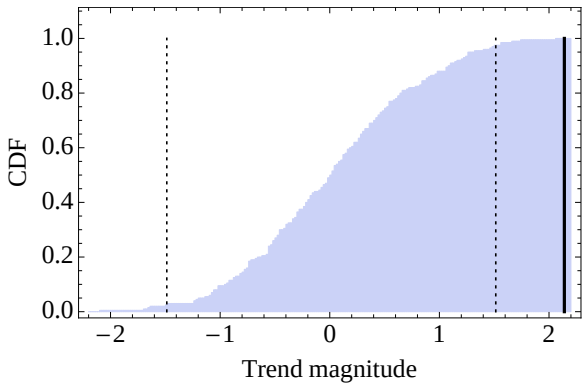

Figure 5.24: *Cumulative distribution of linear trends, calculated from 200 realizations of fGns with H=0.91. The area within the dashed lines represent a 95% confidence interval, where trends may occur by chance. The thick black line represents the linear trend from Reykjanes Ridge, with normalized magnitude 2.14*

From figure 5.24, the linear trend is significant by the LRM null hypothesis.

5.3.2 Vøring Plateau

The QQ-plot in figure 5.25 shows that a normal distribution fit the SST paleodata from the Vøring Plateau well:

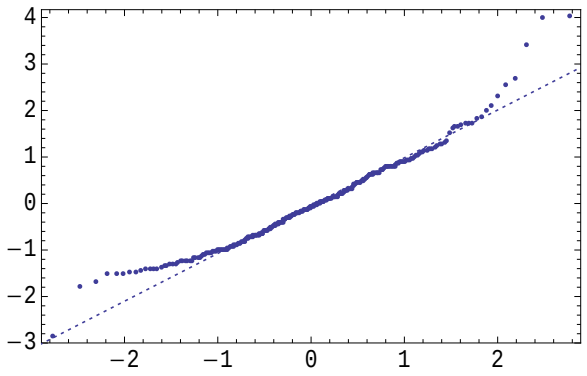

Figure 5.25: *Quantile deviation for Vøring Plateau paleo data from a normal distribution*

ML estimate of H from paleo data: H=0.84, β=0.64.

By Monte Carlo simulation, 50 realizations of fGns with H=0.84 are generated numerically. The likelihood functions are presented in figure 5.26. The ML estimate probabilities of H for the 50 realizations are shown in figure 5.27.

The standard deviation of the estimates: σ=0.023

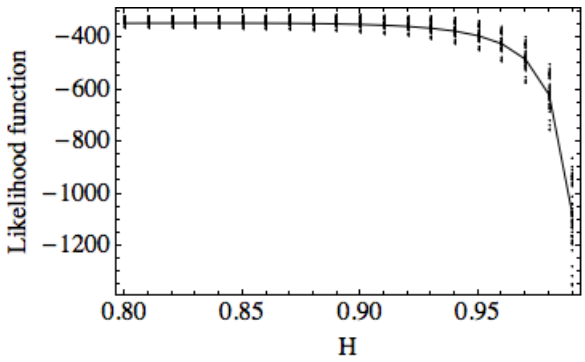

Figure 5.26: *Likelihood functions for H are shown as error bars for the 50 realizations of fGns with prescribed H=0.84. The solid line is the mean likelihood function*

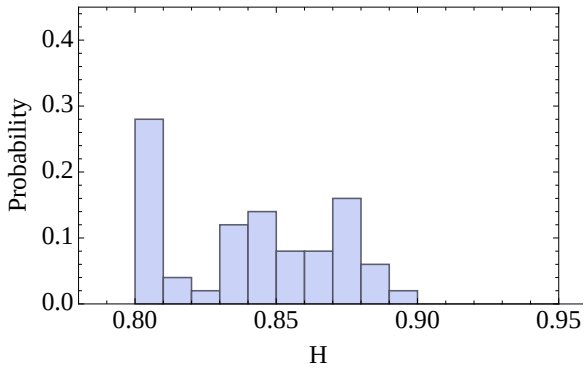

Figure 5.27: *Probability distribution of H estimates*

The significance of the linear trend found in the paleo time series is estimated from a Monte Carlo study. Figure 5.28 show probability distribution of linear trends calculated from 200 realizations of fGns with the prescribed memory component H=0.84. The histogram of the CDF of the trends is represented in figure 5.29.

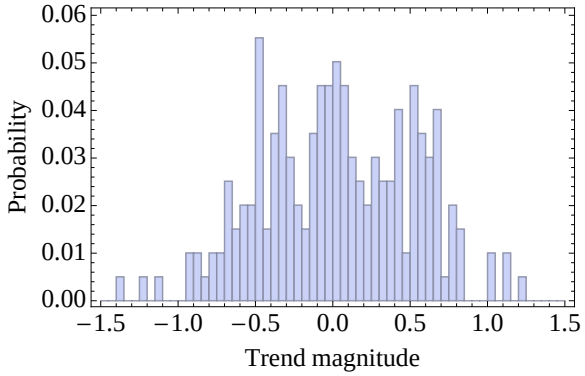

Figure 5.28: *Probability distribution of linear trends calculated from 200 realizations of fGns with H=0.84*

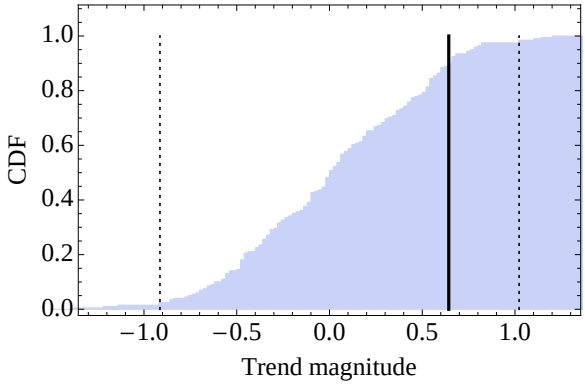

Figure 5.29: *Cumulative distribution of linear trends calculated from 200 realizations of fGns with H=0.84. The area within the dashed lines represent a 95% confidence interval, where trends may occur by chance. The thick black line represents the linear trend from Vøring Plateau, with normalized magnitude 0.643*

From figure 5.29, the linear trend is not significant by the LRM null hypothesis.

Chapter 6

Discussion

In this thesis, simulated and paleoproxy SST time series have been analyzed for multiple purposes. The memory properties in regional and Hemispheric model time series are elaborated, where 5 different climate models are used and all together 12 experiments taken into account. Among the models we find both GCMs and models of intermediate complexity, with ESM structure or simply coupled AOGCM structure. The set of experiments include both dynamical full-forcing simulations, and control simulations with no or constant forcing. The results from the LRM analysis show that all except two Hemispheric SST records have stronger LRM than regional records, and that one of the SST time series is better described by an AR(1) stochastic process than an fGn process, see section 6.1 for further details.

Linear trends are estimated for regional SST model time series, from Reykjanes Ridge and the Vøring Plateau. The trends are compared with corresponding trends from the sediment core SST signals. The only model experiment exhibiting similar SST development as the paleoproxy data, is the experiment from the CLIMBER-3α model of intermediate complexity. See section 6.2 for further details.

The final study in this thesis involves the use of an LRM hypothesis for the sediment core SST time series. The MLE method is applied to estimate the Hurst exponent from the two time series, resulting in H=0.91 for Reykjanes Ridge and H=0.84 for the Vøring Plateau. A Monte carlo study is performed to estimate the

uncertanties. The significance of the linear "trends" from the fGn time series are tested with the LRM hypothesis, and the results show that only the linear trend at Reykjanes Ridge of 1 °C warming /2800 years is significant. The cooling of 0.3 °C /2800 years found for the Vøring Plateau might occur by chance by the LRM hypothesis. See section 6.3 for further details.

6.1 LRM study

The scaling properties of the (S)ST time series in the wavelet variance, periodogram and variogram vary between the differenet models, but also between regional and Hemispheric data with full forcing or no/constant forcing.
Analysis results from the regional SST records from the models LOVECLIM, CLIMBER-3α, COSMOS full forcing, COSMOS unforced exp., and ECHO-G suggest that the time series are persistent, with a β value between 0.5-1.1. Quasi-periodic oscillatory modes and boundary effects create artifacts in the plots, making it difficult to fit a straight line. It is evident from the figures though, that the records do not exhibit an AR(1)-like behaviour on long time scales. An AR(1) process evolves in time from a Brownian motion to a white noise, and the slopes of the studied time series do not follow this pattern.
The Hemispheric records from LOVECLIM and ECHO-G show even stronger persistence, with β slightly higher than 1. These signals are similar to the
[*Moberg et al.* (2005)] paleoproxy temperature reconstruction. The periodogram, wavelet variance and variogram are smoother than for the regional records from the same model simulations, making it easier to fit a straight line.
The analysis of the NH data from the COSMOS full forcing and unforced simulations provide unusual results. The estimated β is lower than for the regional records, which is inconsistent with the results of all other model simulations in this study. It is also inconsistent with what is found in instrumental records [*Rypdal et al.* (2013), *Fredriksen* (2013)], namely that global surface temperature records are more persistent than local records. The cause of this behaviour is not known. It might be associated with the ENSO-like oscillation observed in the Hemispheric wavelet variance and periodogram.

The HadCM3 record is the only record which is possibly more similar to an AR(1) stochastic process than an fGn. The regional record is similar to an fBm on short time scales, and a pink, (β=1) noise on longer time scales. The Hemispheric record shows the same pattern, but has a β value close to a Brownian motion on the shortest time scales (β=2), and a persistent noise for scales longer than a decade.

To validate that the results from this memory analysis are correct, the modeled (S)ST time series can be analyzed by other statistical methods. Among them we find DFA (detrended fluctuation analysis) and the MLE method. The results would also be improved if the techniques for detrending climate signals were better. The method applied here involves finding the best polynomial fit for detrending, and only detrend a signal if the periodogram of the detrended signal is similar to an fGn statistical model. Improvement of detrending techniques is a topic for future work, that will improve the β estimates from the wavelet variance, the periodogram and the variogram. At last, analyzing a wider selection of climate model experiments is also important for validation, in order to improve the statistical uncertanties.

6.2 Linear trend analysis

When analyzing linear trends in the model time series, the CLIMBER experiment is the only realization which exhibit antiphased linear trends for Reykjanes Ridge and the Vøring Plateau. The other models either show no trends at all, or trends only in one of the two locations. Whatever mechanism driving the antiphasing in the paleo data, it is not incorporated into these models.

Before studying the mechanisms of the CLIMBER model in search of an explanation to the antiphasing between eastern and western North Atlantic, more realizations from the model should be analyzed. The antiphasing might be a coincidence, so an ensemble should be analyzed where initial conditions vary. If the trends are still significant, then there most likely exist some internal variability in the model

that causes this.

Reproduction of the MWP and LIA in model simulations is good for some experiments. COSMOS fails to reproduce this variability in 6 out of 7 full forcing experiments, and it is not clear from exp. Erik2 by ECHO-G either. For the remaining experiments that are analyzed, a positive SST anomaly is detected during the MWP, and a negative anomaly is detected during the LIA. The CLIMBER model is the only one showing antiphasing of the events between Reykjanes Ridge and the Vøring Plateau, similar to the sediment core SST time series.
The varying degree of reproduction of the (possibly) forcing-induced climate anomalies from the simulated SST time series, can be explained in the following way. First, the data input for external forcing was not the same for all models. Another reason is that the models incorporate the forcing differently. Responses and feedbacks are more complex in GCMs than in thermodynamic or statistic-dynamical models, and interaction with the biosphere and ice sheets in an ESM also produce different outputs than an atmosphere-ocean coupled model.

From the time series figures in sect. 3.1.1 and 5.2.1, observe that the simulated SST ranges for Reykjanes Ridge and the Vøring Plateau deviate from the sediment core SST temperature. This is due to model configurations, and has little implications for this study. If polar regions were involved on the other hand, one must be more careful. The sea ice extent on low latitudes will differ from the true extent, and produces obvious errors in sea ice reconstruction studies.

It must also be taken into consideration that there are uncertainties in paleorpxy based reconstructions associated with core dating and processing techniques, as well as methods to convert diatom assemblages into past surface temperature estimates.

6.3 Model performance partial assessment

The studies performed in this thesis on reconstructed paleoproxy ST time series and climate model ST time series, give an indication of the model's ability to reproduce LRM, linear trends and known anomalies from ST records. Areas considered include the subpolar Noth Atlantic and the Northern Hemisphere, so the assessment only cover these regions.

Table 6.1 shows the simplified configuration of the models:

Model	**ESM**	**complexity**
LOVECLIM	yes	intermediate
CLIMBER-3α	yes	intermediate
COSMOS	yes	GCM
ECHO-G	no	GCM
HadCM-3	no	GCM

Table 6.1: *Configuration of climate models under study.*

Table 6.2 shows the overall results for the models, based on the criteria given in *, ** and ***:

* LRM properties detected on long time scales for both regional and Hemispheric ST record. (Or only for the regional record, for the CLIMBER-3α where Hemispheric data are unavailable.

** Significant and antiphased linear trends in SST found for Reykjanes Ridge and Vøring Plateau.

*** MWP and LIA detected and antiphased for Reykjanes Ridge and the Vøring Plateau.

Model	**LRM***	**Trends****	**Anomalies*****
LOVECLIM	yes	no	no
CLIMBER-3α	yes	yes	yes
COSMOS	yes	no	no
ECHO-G	yes	no	no
HadCM-3	no	no	no

Table 6.2: *Results for model time series analysis of LRM, linear trends and ST anomalies*

The CLIMBER-3α performs overall best in the three studies mentioned above. This model is of intermediate complexity, so the degree of complexity is not proportional to the ability to reproduce past climate. table 6.2 also shows that all ESMs display LRM properties on long time scales, suggesting that such LRM is associated with slow feedbacks that are only well modeled by introducing Earth system components that go beyond the AOGCMs.

6.4 LRM null hypothesis applied to regional paleo climate data

Quantile plots for the sediment core SST time series from Reykjanes Ridge and the Vøring Plateau, show that the assumption of a normal distribution for the data sets is reasonable. By linear regression, the linear trend magnitudes in the SST time series are calculated for the two regions. The Monte Carlo study shows that the linear trend detected at Reykjanes Ridge is significant, but not the trend at the Vøring Plateau. This is a deviation from the results obtained when applying a white noise null hypothesis, claiming that both linear trends are significant.
This contradiction in a simple trend study is only one example of the implications associated with choosing an LRM model instead of an AR(1) model for climate signal analysis. Elaborating the implications and consequences for future climate changes is another part of the future work on climate and LRM properties. Some work has already been done on this topic. The general idea in

[*Rypdal & Rypdal* (2013)] is that the increase in surface temperature will be even greater than anticipated, due to LRM effects in the slowly responding subsystems in the climate system.

Chapter 7

Conclusion

In this thesis, surface temperature data from paleoclimate reconstructions, as well as model simulations are analyzed. The first task was to study persistence in regional and Hemispheric ST records from the climate models. The results indicate that simulated ST from three models follow the same pattern as observed and reconstructed ST records. The ST timeseries from the models LOVECLIM, CLIMBER-3α, and ECHO-G are persistent, and Hemispheric records have stronger LRM than regional records. Analysis of ST records from the COSMOS model show weaker persistence for Hemispheric data. The HadCM3 Hemispheric ST times series seems to be best described by an AR(1) stochastic process, although this simulation also retains some persistence on the long time scales.
The second study of the thesis involves estimating linear trends in regional SST time series from paleoproxy reconstructions and model simulations. Results show that only the CLIMBER-3α model reproduces the antiphased linear trends observed from the reconstructed SST timeseries. The MWP and LIA were reproduced in most of the studied regional SST time series from model simulations, the exception was the COSMOS model, where the anomalies were only detected in 1 out of 7 experiments.
The conclusion on model performance from the studies in this thesis, is that the simulation from the CLIMBER-3α climate model performs best in reproducing LRM, linear trends and known anomalies in ST in the North Atlantic realm.
The final task was to estimate the Hurst exponent for the regional paleoproxy SST

data, with a hypothesis of LRM in the timeseries. The MLE method was used to estimate H=0.91 for the Reykjanes Ridge, and H=0.84 for the Vøring Plateau. Linear trends of the reconstructed time series were estimated by linear regression, and the significance of the trends were estimated by a Monte Carlo study. Only the warming trend of 1 °C/2800 years at Reykjanes Ridge was found to be significant.

Chapter 8

Bibliography

[*Andersen et al.* (2004)] Andersen, C., N. Koç, A. Jennings, J. T. Andrews, (2004): "Nonuniform response of the major surface currents in the Nordic Seas to insolation forcing: Implications for the Holocene climate variability", *Paleoceanography*, volume 19, PA000873.

[*Berner et al.* (2011)] Berner, K. S., N. Koç, F. Godtliebsen, D. Divine, (2011): "Holocene climate variability of the Norwegian Atlantic Current during high and low solar insolation forcing", *Paleoceanography*, volume 26, PA2220.

[*Berner et al.* (2008)] Berner, K. S., N. Koç, D. Divine, F. Godtliebsen, M. Moros, (2008): "A decadal-scale Holocene sea surface temperature record from the subpolar North Atlantic constructed using diatoms and statistics and its relation to other climate parameters", *Paleoceanography*, volume 23, PA2210.

[*Chardhuri & Marron* (1999)] Chardhuri, P., and J. S. Marron (1999): "SiZer for exploration of structures in curves", *J. Am. Stat. Assoc.*, volume 94, pp 807–823.

[*Collins et al.* (2001)] Collins, M., S. F. B. Tett, C. Cooper, 2001: "The internal climate variability of HadCM3, a version of the Hadley Centre coupled climate model without flux adjustments", *Clim. Dyn.* volume 17, pp. 61-81.

[*Devore & Peck* (1990)] Devore, J., R. Peck, 1990: "Introductory statistics", West Publishing Company, St. Paul. MN, USA.

[*Fredriksen* (2013)] Fredriksen, H.-B., 2013: "Long-range memory in Earth surface temperatures: Spatial scale dependence and land-sea differences", Master thesis, University of Tromsø, Norway.

[*Gonzàlez-Rouco et al.* (2003)] Gonzàlez-Rouco, F., H von Storch, E. Zorita, 2003: "Deep soil temperature as proxy for surface-air temperature in a coupled model simulation of the last thousand years", *Geophys. Res. Lett.* volume 30, no 21, 2116.

[*Gonzàlez-Rouco et al.* (2006)] Gonzalez-Rouco, J. F., H. Beltrami, E. Zorita, H. von Storch, 2006: "Simulation and inversion of borehole temperature profiles in surrogate climates: spatial distribution and surface coupling", *Geophys. Res. Lett.* volume 33, L01703.

[*Goosse et al.* (2010] Goosse, H., V. Brovkin, T. Fichefet, R. Haarsma, P. Huybrechts, J. Jongma, A. Mouchet, F. Selten, P.-Y. Barriat, J.-M. Campin, E. Deleersnijder, E. Driesschaert, H. Goelzer, I. Janssens, M.-F. Loutre, M. A. Morales Maqueda, T. Opsteegh, P.-P. Mathieu, G. Munhoven, E. J. Pettersson, H. Renssen, D. M. Roche, M. Schaeffer, B. Tartinville, A. Timmermann, S. L. Weber, (2010): "Description of the Earth system model of intermediate complexity LOVECLIM version 1.2", *Geoscientific Model Development*, volume 3, pp. 603-633.

[*Goosse et al.* (2010)] Goosse, H., E. Crespin, S. Dubinkina, M.-F. Loutre, M. E. Mann, H. Renssen, Y. Sallaz-Damaz, D. Shindell, (2010): "The role of forcing and internal dynamics in explaining the "Medieval Climate Anomaly"", *Climate Dynamics*, volume 39, pp. 2847-2866.

[*Gordon et al.* (2000)] Gordon, C., C. Cooper, C. A. Senior, H. Banks, J. M. Gregory, T. C. Johns, J. F. B. Mitchell, R. A. Wood, 2000: "The simulation of SST, sea ice extents and ocean heat transports in a version of the Hadley Centre coupled model without flux adjustments", *Clim. Dyn.* volume 16, pp 147-168.

[*Hasselmann* (1976)] Hasselmann, K., 1976: "Stochastic climate models Part I. Theory", *Tellus*, volume 28, pp. 473-485.

[*Imbrie & Kipp* (1971)] Imbrie, J., N. G. Kipp, (1971): "A new micropalentological method for quantitative micropalentology: Application to late Pleistocene Caribbean core", in *Late Cenozoic Glacial Ages*, pp. 71-181, Yale Univ. Press, New York, NY, USA

[*IPCC* (2007)] Randall, D. A., R. A: Wood, S. Bony, R. Colman, T. Fichefet, J. Fyfe, V. Kattsov, A. Pitman, J. Shukla, J. Srinivasan, R. J. Stouffer, A. Sumi, K. E. Taylor, 2007: "Climate Models and Their Evaluation. In: Climate Change 2007: The Physical Science Basis. Contributions of Working Group 1 to the Fourth Assessment Report of the Intergovermental Panel on Climate Change [Solomon, S., D. Qin, Manning, M., Chen, Z., Marquis, M., Averyt, K. B., Tignor, M. and Miller, H. L.(eds)]. pp. 589-664. Cambridge University Press, Cambridge, UK and New York, NY, USA.

[*Jungclaus et al.* (2010)] Jungclaus, J. H., C. Timmreck, C. H. Reick, V. Brovkin, K. Six, J. Segschneider, M. A. Giorgetta, T. J. Crowley, J. Pongratz, N. A. Krivova, L. E. Vieira, S. K. Solanki, D. Klocke, M. Botzet, M. Esch, V. Gayler, H. Haak, T. J. Raddatz, E. Roeckner, R. Schnur, H. Widmann, M. Claussen, B. Stevens, J. Marotzke, (2010): "Climate and carbon-cycle variability over the last millenium", *Climate of the Past*, volume 6, pp. 723-737.

[*Koç Karpuz & Schrader* (1990)] Koç Karpuz, N., H. Schraeder, (1990): "Surface sediment diatom distribution and Holocene paleotemperature variations in the Greenland, Iceland and Norwegian Sea", *Paleoceanography*, volume 5, pp. 557-580.

[*Malamud & Turcotte* (1998)] Malamud, B. D., D. L. Turcotte, 1998: "Self-affine time series: measures of weak and strong persistence", *Journal of Statistical Planning and Infernece*, volume 80, pp. 173-196.

[*Mann et al.* (2009)] Mann M. E., Z. Zhang, S. Rutherford, R. S. Bradley, M. K. Hughes, D. Shindell, C. Ammann, G. Faluvegi, F. Ni, (2009): "Global signatures and dynamical origins of the Little Ice Age and Medieval Climate Anomaly", *Science* volume 326, pp. 1256–1260.

[*McLeod et al.* (2007)] McLeod, I. A., H. Yu, Z. L. Krougly, 2007: "Algorithms for Linear Time Series Analysis: With R Package". *Journal of Statistical Software*, volume 23 issue 5, pp. 1–26.

[*Mengel et al.* (2012)] Mengel, M., A. Levermann, C.-F. Schleussner, A: Born, 2012: " Enhanced Atlantic subpolar gyre variability through baroclinic threshold in a coarse resolution model",*Earth Syst. Dynam.* volume 3, pp. 189-197.

[*Miettinen et al.* (2012)] Miettinen, A., D. Divine, N. Koc, F. Godtliebsen, I. R. Hall, 2011: "Multicentennial Variability of the Sea Surface Temperature Gradient across the Subpolar North Atlantic over the Last 2.8 kyr", *J. Climate*, volume 25, pp. 4205-4219.

[*Moberg et al.* (2005)] Moberg, A., D. M. Sonechkin, K. Holmgren, N. M. Datsenko, W. Karlén, 2005: "Highly variable Northern Hemisphere temperatures reconstructed from low and high-resolution proxy data", *Nature* volume 433, pp. 613-617.

[*Montoya et al.* (2005)] Montoya, M., A. Griesel, A. Levermann, J. Mignot, M. Hofmann, A. Ganopolski, S. Rahmstorf, 2005: "The earth system model of intermediate complexity CLIMBER-3α. Part 1: description and performance for present-day conditions", *Clim. Dyn*, volume 25, pp 237-263.

[*Pelletier and Turcotte* (1999)] Pelletier, J. D., D. Turcotte, 1999: "Self-affine time series: II. Applications and models", *Adv. geophys*, volume 10, pp. 91-166.

[*Qian* (2003)] Qian, H., 2003: "Fractional Brownian Motion and Fractional Gaussian Noise", pp. 22-33, Springer-Verlag, Berlin Heidelberg, Germany.

[*Schleussner & Feulner* (2012)] Schleussner, C.-F., G. Feulner, 2012: A volcanically triggered regime shift in the subpolar North Atlantic ocean as a possible origin of the Little Ice Age", *Clim. Past Discuss* volume 8, 6199-6219.

[*Rybski et al.* (2006)] Rybski, D., A. Bunde, S. Havlin, H. von Storch, 2006: " Long term persistence in climate and the detection problem", *Geophysical. Res. Lett.* volume 33, L06718.

[*Rypdal & Rypdal* (2010)] Rypdal. M., K. Rypdal, 2010: "Testing hypotheses about sun-climate complexity inking", *Phys. rev. Lett.*, volume 104, 128501

[*Rypdal et al.* (2013)] Rypdal, K., L. Østvand, M. Rypdal, 2013: "Long-range memory in Earth's global temperature on time scales from months to centuries", *J. Geophys. Res. Atmos*, doi: 10.1002/jgrd.50399.

[*Rypdal & Rypdal* (2013)] Rypdal, M., K. Rypdal, 2013: "Long-memory effects in linear-response models of Earth's temperature and implications for future global warming", submitted to *J. Climate*, http://arxiv.org/pdf/1305.5080v1.pdf

[*Saltzman* (2002)] Saltzman, B. 2002: "Dynamical Paleoclimatology. Generalized Theory of Global Climate Change", Academic Press, San Diego, California, USA and London, UK.

[*Schrader & Gersonde* (1978)] Schrader, H. J., and R. Gersonde, 1978: "Diatoms and Silico-flagellates. Micropalentological counting methods and techniques - An exercise on an eight meters section of the lower Pliocene of Capo Rossello", *Utrecht Micropalentol. Bull.*, volume 17, pp. 129-176.

[*ter Braak & Juggins* (1993)] ter Braak, C. J. F., S. Juggins, 1993: "Weighted averaging partial least squares regression (WA-PLS); An improved method for reconstructing environmental variables from species assemblages", *Hydrobiologia*, volume 269-270, pp. 485-502.

[*Torrence & Compo* (1998)] Torrence, C., G. P. Compo, 1998: "A Practical Guide to Wavelet Analysis", *Bull. Amer. Met. Soc.*, volume 79, pp. 61-78.

[*Vivero & Health* (2010)] Vivero O., W. P. Health, 2010: "Regularised Estimators for ractional Gaussian Noise", *Proceedings of the 49th IEEE Conference on Decision and Control*, pp. 5025-5030, 2010a.

[*von Storch et al.* (2004)] von Storch, H., E. Zorita, J. M. Jones, Y. Dmitriev, S. F. B. Tett, 2004: "Reconstructing past climate from noisy data", *Science* volume 304, pp. 679-682.

[*Walpole et al.* (2007)] Walpole, R. E., R. H. Myers, S. L. Myers, K. Ye, 2007: "Probability and statistics for engineers & scientists", pp. 310-315, Pearson Education Inc. Upper Saddle River, New Jersey, USA.

[*Wefer et al.* (2003)] Wefer, G., D. Billet, D. Hebbeln, B. B. Jorgensen, M. Schlüter, T. C. E. Van Weering, 2003: "Ocean Margin Systems", pp. 57-66, Springer Verlag, New York, NY, USA.

[*Zhang et al.* (2005] Zhang, Y., A. B. Baggeroer, J. G. Bellingham, 2005: "The Total Variance of a Periodogram-Based Spectral Estimate of a Stochastic Process With Spectral Uncertainty and its Application to Classifier Design", *IEEE transactions on signal processing*, volume 53, issue 12, pp. 4556-4567.

Appendix A

Area of grid

At latitude θ we have an infinitismal area:

$$\mathrm{dA} = \mathrm{dl} \cdot \mathrm{db} = \mathrm{r}^2 \, \mathrm{d}\theta \, \mathrm{d}\varphi \, \cos(\theta)$$

Where dl is an infinitesmal length element in longitudinal direction and db is an infinitesmal length element in latitudinal direction.
Grid area with $\Delta\theta \cdot \Delta\varphi$ degrees:

$$\Delta\mathrm{A} = \int_{\varphi_0}^{\varphi_0+\Delta\varphi} \int_{\theta_0}^{\theta_0+\Delta\theta} \mathrm{r}^2 \, \cos(\theta) \, \mathrm{d}\theta \, \mathrm{d}\varphi \, = \Delta\varphi \, \mathrm{r}^2 \, [\sin(\theta_0 + \Delta\theta) \, - \sin(\theta_0] \qquad \text{(A.1)}$$

The mean Earth radius used is r=6367 km.